A cis-acting mechanism mediates transcriptional memory at Polycomb target genes in mammals

Daniel Holoch, Michel Wassef, Cecilia Lövkvist, Dina Zielinski, Setareh Aflaki, Bérangère Lombard, Tiphaine Héry, Damarys Loew, Martin Howard, Raphaël Margueron

HAL Id: hal-03448602

https://hal.sorbonne-universite.fr/hal-03448602

Submitted on 25 Nov 2021

A *cis*-acting mechanism mediates transcriptional memory at Polycomb target genes in mammals

Daniel Holoch[1,2,7], Michel Wassef[1,2,7], Cecilia Lövkvist[3,4*], Dina Zielinski[1,2,5], Setareh Aflaki[1,2], Bérangère Lombard[1,6], Tiphaine Héry[1,2], Damarys Loew[1,6], Martin Howard[3] & Raphaël Margueron[1,2*]

[1] Institut Curie, Paris Sciences et Lettres Research University, Sorbonne University, 75005 Paris, France. [2] INSERM U934/CNRS UMR 3215, 75005 Paris, France. [3] John Innes Centre, Norwich Research Park, Norwich NR4 7UH, United Kingdom. [4] Present address: Biotech Research and Innovation Centre, University of Copenhagen, 2200 Copenhagen N, Denmark, [5] INSERM U900, Mines ParisTech, 75005 Paris, France. [6] Proteomics Mass Spectrometry Laboratory, 75005 Paris, France. [7] These authors contributed equally: Daniel Holoch, Michel Wassef. *e-mail: cecilia.loevkvist@bric.ku.dk, raphael.margueron@curie.fr.

Abstract

Epigenetic inheritance of gene expression states enables a single genome to maintain distinct cellular identities. How histone modifications contribute to this process remains unclear. Using global chromatin perturbations and local, time-controlled modulation of transcription, we establish the existence of epigenetic memory of transcriptional activation for genes that can be silenced by the Polycomb group. This property emerges during cell differentiation and allows genes to be stably switched following a transient transcriptional stimulus. This transcriptional memory state at Polycomb targets operates in *cis*; however, rather than relying solely on read-and-write propagation of histone modifications, the memory is also linked to the strength of activating inputs opposing Polycomb proteins and therefore varies with the cellular context. Our data and computational simulations suggest a model whereby transcriptional memory arises from double-negative feedback between Polycomb-mediated silencing and active transcription. Transcriptional memory at Polycomb targets thus depends not only on histone modifications but also on the gene-regulatory network and underlying identity of a cell.

Introduction

Epigenetic memory, generally understood to designate a long-lived change in gene expression in response to a short-lived signal, plays a critical role in ensuring the stability of functionally specialized cell types. Epigenetic information can be transmitted through cell divisions via *cis*- or *trans*-acting mechanisms [1-4]. The persistence of epigenetic memory in *cis* has been proposed to rely on semi-conservative read-and-write mechanisms that faithfully copy covalent modifications to DNA and histones concurrently with genome replication [1]. While direct evidence indicates that DNA methylation carries epigenetic information according to this logic [5-7], it has remained controversial whether histone modifications can function similarly in the absence of enabling mutations or short-interfering-RNA-driven feedbacks [8-14].

We examined this question using mammalian Polycomb group proteins as a model. Polycomb proteins play a key role in silencing developmental genes outside of their normal spatial domains of expression [15,16]. By extension from studies of *Drosophila* and plants [17-21], it is widely taken for granted that the Polycomb machinery mediates a chromatin-based epigenetic memory of the silent state in mammals, but an unequivocal test of this hypothesis has been lacking. Furthermore, if such a memory indeed exists, there is much debate regarding its mechanistic basis. The Polycomb system is endowed with the key properties required for a semi-conservative mode of epigenetic propagation: histone H3 lysine 27 trimethylation (H3K27me3) catalyzed by Polycomb Repressive Complex 2 (PRC2) is distributed in a semi-conservative pattern following replication [22] and PRC2 activity is directly stimulated by H3K27me3 [23,24]. However, recent reports have shown that, outside of *C. elegans* [25], the mark is neither necessary [26-28] nor sufficient [9,11,29] to instruct its own propagation. We therefore sought to clarify whether and how the Polycomb machinery might confer epigenetic memory of transcriptional states in mammalian cells.

Results

Temporary disruption of PRC2 activity results in irreversible transcriptional changes at many PRC2 target genes.

We reasoned that if Polycomb proteins were simply transcriptional repressors with no role in transcriptional memory, then any changes arising from inhibition of their activity would be fully reversed once that inhibition were lifted. Conversely, if Polycomb proteins acted not only to repress transcription but also to maintain a memory of transcription states, a temporary perturbation of their activity would be expected to result in a permanent disruption of that memory. To test this idea we treated cultured mouse neural progenitor cells (NPCs) with two mechanistically orthogonal pharmacological inhibitors of PRC2 [30,31] for 15 population doublings (14 days) until H3K27me3 became undetectable, and subsequently cultured the cells for 20 additional population doublings (15 days) in the absence of inhibitors until global H3K27me3 was fully recovered (Fig. 1a, Extended Data Fig. 1a-d and Extended Data Table 1). This strategy allowed us to assess whether temporary disruption of PRC2 activity triggers enduring changes in the transcriptome and in H3K27me3 localization. Importantly, temporary PRC2 inhibition did not result in any major or lasting phenotypic changes in NPC clonal growth, cell cycle, apoptosis or differentiation capacity (Extended Data Fig. 1e-i), and expression signatures of NPC markers were maintained (Extended Data Fig. 2a-c).

We first surveyed the overall landscape of H3K27me3 enrichment across the genome. In agreement with recent studies of mouse embryonic stem cells (mESCs) [26-28], we found that, with notable exceptions described further below, PRC2 could re-establish H3K27me3 patterns *de novo* with high fidelity genome-wide in NPCs (Fig. 1b and Extended Data Fig. 2d), indicating that the information provided by the position of pre-existing H3K27me3 is largely dispensable for proper localization of PRC2 activity.

A contrast emerged between NPCs and mESCs, however, when we specifically examined transcriptional changes at putative direct PRC2 target genes, defined by the presence of a H3K27me3 peak at their transcription start site (TSS). Consistent with previous work [32-35], the majority of presumed PRC2 targets were not significantly upregulated in the presence of PRC2 inhibitors (Extended Data Fig. 3a). We found by examining ATAC-seq experiments previously conducted on the same clone of NPCs [36] that the genes that do go on to become de-repressed upon inhibitor treatment tend to possess more highly accessible chromatin around their TSS (Extended Data Fig. 3b), suggesting that they might be poised to become activated by transcriptional activators. Among these 305 upregulated target genes in NPCs, we observed two distinct responses: genes that returned to a repressed state upon inhibitor washout (*reversible*), and genes that remained expressed on a permanent basis (*irreversible*), which was accompanied by incomplete recovery of local H3K27me3 (Fig. 1c-e, and Extended Data Fig. 2e). These irreversible PRC2 targets attest to the existence of an epigenetic transcriptional switch insofar as their active expression state far outlasts the initial causative event and is stable through many cell cycles. The widespread occurrence of such a memory of active transcription at PRC2-regulated genes in NPCs differs sharply from what we observed in mESCs that we subjected to the same procedure, in which changes in gene expression at H3K27me3-positive genes (identified using recently published ChIP-seq data [26]) were entirely reversed upon PRC2 inhibitor washout (Fig. 1f and Extended Data Fig. 3a,c,d), consistent with an earlier report [26].

In order to determine whether transcriptional memory of Polycomb target genes is a specific feature of NPCs or whether it is also present in other differentiated cell types, we analyzed two independently derived lines of immortalized mouse embryonic fibroblasts (iMEFs "A" and "B"). While iMEF B cells underwent the same PRC2 inhibition and washout treatment as the NPCs and mESCs (Extended Data Fig. 3e), we also separately deleted and subsequently re-introduced *Ezh2* in both iMEF A and B. ATAC-

seq performed on iMEF A cells again revealed a higher degree of chromatin accessibility near the TSS of those H3K27me3-marked genes that would become de-repressed once PRC2 was disrupted (Extended Data Fig. 3a,b). In both iMEF lines we once again found numerous genes subject to epigenetic switching, in proportions comparable to those observed in NPCs (Fig. 1f and Extended Data Fig. 3f-h; [34]). Similarly to reversible genes and to H3K27me3-positive genes overall, irreversible genes are enriched for development-related gene ontologies across the three cell lines (Extended Data Fig. 4). Many of these genes encode transcription factors (TFs) known to act as key cell fate regulators. Correspondingly, when we assessed changes in chromatin accessibility between wild-type and *Ezh2*-rescue iMEF A cells, we could identify 310 ATAC-seq peaks that are gained irreversibly, and among the motifs determined to be significantly enriched in these regions we found a number of recognition sites for TFs encoded by irreversibly switched loci, including Hox genes (Extended Data Fig. 5a-c and Extended Data Table 2). Interestingly, we found several instances of genes that were repressed in one iMEF cell line while active in the other, and which, upon release of PRC2-mediated repression, reached comparable transcript levels in both cell lines (Extended Data Fig. 6a). This similarity in transcript abundance suggests that the epigenetic switch in expression states resulting from transient loss of PRC2 is of a biologically relevant magnitude. Altogether, these observations suggest that transcriptional memory of activation is a widespread developmental feature of PRC2 target genes that is absent from pluripotent stem cells and emerges during cell differentiation.

We also noticed individual genes that exhibited distinct reversible and irreversible responses to transient disruption of PRC2 activity in different cell lines. While certain targets displayed a lasting memory of activation in both iMEF A and iMEF B (e.g., *Hoxb6*), others behaved irreversibly in one iMEF line but were either reversible (e.g., *Axin2*) or simply unresponsive to *Ezh2* deletion (e.g., *Lin28b*) in the other (Extended Data Fig. 6b). These results indicate that the ability of specific PRC2 target

genes to exhibit transcriptional memory of activation is not an intrinsic property of those genes but rather depends on elements of the cellular context such as cell-type-specific activating or repressive TFs. Since cultured fibroblasts are known to retain a positional memory of their site of origin in the organism [37], these differential manifestations of transcriptional memory may reflect features of the anatomical regions from which they were initially isolated.

Taken together, these data indicate that epigenetic memory for PRC2 target genes does not solely rely on a read-and-write mechanism involving the H3K27me3 mark. Indeed, in such a scenario any locus losing H3K27me3 even temporarily should remain perpetually released from PRC2 targeting, a prediction refuted by the general dispensability of H3K27me3 for *de novo* localization of PRC2 activity (Fig. 1b; [26-28]), by the existence of reversible genes and by the variable susceptibility of individual genes to epigenetic memory depending on the cellular context. We infer from these observations that read-and-write dynamics alone cannot account for the memory of transcriptional states at PRC2 target genes, and that additional principles must also contribute.

Epigenetic memory at PRC2 target genes is associated with a mutual antagonism between PRC2 activity and transcriptional inputs.

To further elucidate the determinants of heritable activation of PRC2 targets, we examined all individual cases of genes that were de-repressed reversibly in one cell line and irreversibly in another. Strikingly, transcript levels measured by RNA-seq under conditions of PRC2 disruption were significantly higher in the cell line in which they responded irreversibly (Fig. 2a,b). We then conducted comparisons between the full categories of reversible and irreversible targets within each cell line. We found that, upon disruption of PRC2, irreversible gene transcript levels were again significantly higher than those of their reversible counterparts, a trend that held true in every cell line analyzed (Fig. 2c).

In order to investigate whether these higher messenger RNA levels might reflect a more active transcriptional regime, we carried out genome-wide analysis of nascent transcription, chromatin accessibility and profiles of RNA polymerase II (RNA Pol II) and the transcription-coupled modifications H3K4me3 and H3K36me3 in *Ezh2* KO iMEF A cells. We also mapped genome-wide patterns of DNA methylation, a modification whose *de novo* deposition is known to be targeted to the bodies of transcribed genes [38]. While there was no significant difference between reversible and irreversible genes for chromatin accessibility, RNA Pol II or H3K4me3, a mark deposited at active or poised promoters, we found that H3K36me3, which is associated with transcriptional elongation, was much more enriched over irreversible genes than over reversible genes, and this was accompanied by higher levels of nascent transcripts and gene body DNA methylation (Fig. 2d and Extended Data Fig. 7a,b). There was a notable correlation between H3K36me3 enrichment and DNA methylation over individual genes, consistent with a common co-transcriptional origin for these marks and with their reported functional crosstalk [38,39] (Extended Data Fig. 7c).

Collectively, these observations suggest that transcriptional memory at PRC2 target genes may result from high transcriptional activation inputs that prevent re-establishment of PRC2-mediated silencing. In keeping with this idea, while Polycomb proteins inhibit transcription, active transcription is conversely known to antagonize Polycomb activity [40,41], possibly through H3K27 demethylation [42,43] and acetylation [44,45], nucleosome exchange [46,47], the ability of nascent RNA to impede PRC2 association with chromatin [48,49] and through the deposition of histone marks such as H3K4me3 and H3K36me3 that inhibit PRC2 catalytic activity [50,51]. The association we have uncovered between epigenetic switching behavior and the strength of transcriptional activation that Polycomb proteins must counteract therefore suggests that transcriptional memory hinges in part on a dual negative feedback between Polycomb-mediated silencing and active transcription.

A theoretical formalism we recently published predicted that this mutual antagonism is an essential ingredient, together with H3K27 methylation read-and-write feedbacks, for a bistable *cis*-acting memory of transcriptional states at PRC2 target genes[52,53]. Two key parameters in this model are the strength of transcriptional activation, α, and the strength of local PRC2 activity, β. α is modulated by the factors available in a given cell type to influence transcription of a target gene through binding to promoter and enhancer elements. β varies according to the ability of the underlying sequence to recruit PRC2 and facultative subunits that modulate its catalytic output, a property linked to CpG islands for example [54-56] (Fig. 3a). These two parameters are postulated to vary among different PRC2 target genes and cell types. We therefore used this model to perform computational simulations of our PRC2 disruption and rescue experiments and asked whether this would produce behaviors similar to those described above. The result, shown in Fig. 3b, indeed reveals specific combinations of values assumed by α and β that are expected to result in reversible (Fig. 3b, e.g., blue circle) or irreversible (Fig. 3b, e.g., red circle) outcomes. Irreversible switching from repressed to active transcriptional states was robust to declines in the rate of cell division (Extended Data Fig. 7d) such as those we observed in PRC2i-treated cells (Extended Data Fig. 1a). Thus, our experimental observations are compatible with a double-negative feedback between transcription and PRC2 activity as a core theoretical principle. Interestingly, the simulations correctly predict that transcript levels are collectively higher for irreversible target genes than for reversible targets in PRC2-disrupted cells (Fig. 3c). The simulations also predict a more modest difference in local H3K27me3 abundance in untreated wild-type cells, with higher levels for reversible than for irreversible genes. This difference is apparent in our experimental data, though only statistically significant in one cell line (Extended Data Fig. 7e).

Transient activation of individual PRC2 target genes is sufficient to produce epigenetic memory.

Given the ability of transcription to counteract PRC2, we reasoned that epigenetic switching of irreversible genes in response to an artificial bout of PRC2 disruption might reflect a natural ability of these genes to record any short transcriptional stimulus strong enough to locally inhibit PRC2 activity. In support of this notion, computational simulations indicate that genes whose response to transient PRC2 disruption is irreversible (or reversible) should respond in a similarly irreversible (or reversible) fashion to a transient pulse of strong transcriptional activation (Fig. 3d).

To test this hypothesis, we developed a system to transiently activate individual targets one at a time. We engineered iMEF B cells to encode a doxycycline-inducible dCas9-VPR transcriptional activator protein [57] fused with a mutant FKBP12 that acts as a destabilization domain to prevent spurious expression [58,59]. As expected, dCas9-VPR is detected by Western blot only in the presence of doxycycline and of the destabilization domain ligand Shield-1, and disappears rapidly after removal of these compounds (Fig. 4a). In the presence of sgRNAs targeting the promoter region of a gene of interest, we can readily ask whether temporary induction of transcription results in subsequently stable epigenetic memory (Fig. 4a). Remarkably, we observe such a memory in response to a pulse of activation for several irreversible PRC2 target genes including *Alx1*, *Nr2f1* and *Foxa1*, all of which encode lineage-specific developmental regulators. In these cases, transcript levels remain durably elevated after removal of the inducing signal ("VPR washout," after 9 days, i.e., more than 10 population doublings) compared to their initial repressed state ("VPR OFF," Fig. 4b). It is interesting to note that the quantity of mRNA measured after a repressed target gene is flipped on using the dCas9-VPR system ("VPR washout") is typically in the same range as that produced in *Ezh2* KO cells (Fig. 4b), consistent with the idea that transient induction allows the locus to stably overcome repression by PRC2. Importantly, certain PRC2 target genes such as *Hoxb13* display no

memory of activation, arguing against the possibility that the memory represents a nonspecific effect of the assay (Fig. 4c). Epigenetic memory of transient activation by dCas9-VPR is also evident at the protein level, with Western blots revealing a switch in Nr2f1 and Foxa1 accumulation from undetectable amounts to levels (in "VPR washout") in the range of those found in *Ezh2* KO cells (Fig. 4d). At the chromatin level, H3K27me3 is virtually eliminated from the transiently activated loci (Extended Data Fig. 8a, "VPR washout"). In order to exclude the possibility that these effects are the result of persistent activation by residual dCas9-VPR protein, we deleted the transgene from *Nr2f1* and *Foxa1* VPR washout conditions and confirmed that the memory of expression was maintained at both the protein and mRNA levels (Extended Data Fig. 8b,c). Since removing the transgene required a clone isolation and expansion procedure spanning dozens of cell generations, this result further underscores the longevity of the transcriptional memory for these genes. Altogether, these experiments establish that transcriptional memory of activation is a gene-autonomous attribute that enables PRC2 target genes to record a transient transcriptional stimulus.

Hox genes can exhibit gene-specific or coordinated transcriptional memory.

Among the genes repressed in an *Ezh2*-dependent manner in both iMEF A and iMEF B were several members of the *Hoxb* gene cluster (Extended Data Fig. 6b). Hox genes encode key developmental regulators involved in the specification of antero-posterior identity, and regulation of their expression by Polycomb proteins is conserved across metazoans [15,16]. *Hoxb* genes exhibited varying degrees of epigenetic memory in response to transient activation in the dCas9-VPR assay (Fig. 4c and Extended Data Fig. 9a). By sequencing chromatin-associated nascent RNA from iMEF B cells, we were also able to detect a long transcript that sweeps across a large portion of the *Hoxb* cluster, which we term *long-Hoxb* (Extended Data Fig. 9b), distinct from the recently described short *HoxBlinc* [60]. We found that *long-Hoxb* can retain a stable memory of activation when

targeted with dCas9-VPR (Extended Data Fig. 9b), which led us to wonder what impact its transcription might have on other genes in the cluster. Interestingly, both *Hoxb5* and *Hoxb6*, which lie within the *long-Hoxb* transcription unit, were robustly co-activated with *long-Hoxb* and displayed epigenetic memory of this event, whereas the nearby *Hoxb9*, which *long-Hoxb* does not overlap, did not respond to *long-Hoxb* induction (Extended Data Fig. 9c). Thus, the locus-specific activation assay suggests that a single activation decision involving *long-Hoxb* might in principle suffice to flip the transcriptional configuration of several PRC2 target loci in the *Hoxb* cluster in the course of developmental transitions.

We also used the *long-Hoxb* gene to test the kinetics of epigenetic switching by varying the time of dCas9-VPR-mediated induction prior to a constant 9-day washout. This analysis showed that both near-maximal transcriptional induction and near-maximal conversion to an epigenetically stable expressed state occurred with only 1 day of induction (Extended Data Fig. 10a), illustrating the potentially rapid establishment of a transcriptional memory state in response to a short-lived signal. However, examination of additional PRC2 targets revealed that these kinetics are not universal; although *Alx1* and *Foxa1* could likewise undergo epigenetic switching after a 1-day activation, *Nr2f1* showed only a partial response (Extended Data Fig. 10b, compare to Fig. 4b), which coincided with incomplete removal of H3K27me3 from the locus (Extended Data Fig. 10c). Interestingly, computational simulations of shorter activation times indeed predict varying temporal requirements for complete switching as a function of the strength of activation inputs and local PRC2 activity (Extended Data Fig. 10d).

Transcription-coupled modification pathways are individually dispensable for maintenance of epigenetic memory at PRC2 target genes.

We next took advantage of the dCas9-VPR-based local activation system to test whether specific biochemical events associated with transcription were required for the maintenance of transcriptional memory after transient induction. The significant difference in H3K36me3 enrichment over the gene bodies of irreversible PRC2 targets in *Ezh2* KO cells (Fig. 2d and Extended Data Fig. 7a) prompted us to generate a dCas9-VPR line with a deletion in *Setd2*, which encodes the major H3K36 trimethylation activity in mice [61,62] (Extended Data Fig. 11a). In this background, *Nr2f1* and *Foxa1* remained repressed in an Ezh2-dependent manner, and transient dCas9-VPR-mediated activation of these genes still led to a stable memory of expression at levels roughly equivalent to those observed upon *Ezh2* deletion (Fig. 4e). Likewise, when the H3K27 demethylases encoded by *Utx* and *Jmjd3* [43,63-65] are deleted (Extended Data Fig. 11b), which we conjectured might hinder the maintenance of transcriptional memory at PRC2 target genes, *Nr2f1* and *Foxa1* still remain subject to epigenetic switching upon transient dCas9-VPR-mediated induction to a stable expression state similar to that obtained by deleting *Ezh2* (Fig. 4f). Acetylation of the H3K27 residue is also strongly associated with transcription, and presence of this mark antagonizes and indeed is incompatible with PRC2 activity [44,45]. We thus deleted the histone acetyltransferase *Crebbp*, which led to a substantial reduction in global H3K27 acetylation (Extended Data Fig. 11c) but, similarly to the *Setd2* and *Utx/Jmjd3* deletions, did not prevent epigenetic switching of *Nr2f1* and *Foxa1* following a transient dCas9-VPR-dependent induction (Figure 4g). We conclude that none of these machineries is alone sufficient to account for the long-term maintenance of transcription at PRC2 target genes in response to transient activation, suggesting that transcription-associated processes known to counteract PRC2 display a certain degree of redundancy.

Since we had also observed higher levels of DNA methylation over the bodies of irreversible genes relative to reversible genes in *Ezh2* KO cells (Fig. 2d and Extended Data Fig. 7a,b), we attempted to explore whether DNA methylation might be required to prevent restoration of PRC2-dependent repression and therefore to uphold transcriptional memory of activation at these genes. Treatment with 5-aza-2'-deoxycytidine resulted in a dose-dependent loss of global CpG methylation (Extended Data Fig. 11d), but although this coincided with a modest decline in the expression of irreversible PRC2 targets *Nr2f1* and *Foxa1*, the decrease was not dependent on Ezh2, indicating that it did not reflect a resumption of PRC2-dependent silencing (Extended Data Fig. 11e). These results do not reveal an obvious role for DNA methylation in the maintenance of active transcriptional memory states at transiently activated PRC2 targets. The persistence of epigenetic switching in the absence of Setd2 (Fig. 4e), which is necessary for co-transcriptional *de novo* DNA methylation [38,39], further argues against DNA methylation making a critical contribution.

Transcriptional memory at Polycomb target genes acts in *cis*.

Our data suggest a mechanism for transcriptional memory, consisting of a mutual opposition between Polycomb proteins and active transcription, that operates in *cis*, i.e., independently of secondary feedbacks initiated by proteins encoded by PRC2 target loci. Indeed, our local activation experiments establish the gene-autonomous nature of the transcriptional memory, thereby ruling out the idea that the epigenetic switching events are due to a global reconfiguration of the gene-regulatory network (GRN) upon simultaneous de-repression of multiple TFs. Nevertheless, since many PRC2 target genes including *Nr2f1, Foxa1*, *Alx1* and *Hox* genes encode TFs themselves, it is still possible that the observed memory of their activation relies on the initiation of new feedbacks of *trans*-acting factors (Fig. 5a, top) rather than on a *cis*-acting shift (Fig. 5a, bottom). We sought to distinguish between these two scenarios by first evaluating the

genome-wide impact of our single-gene transient induction assays. This analysis revealed that *Nr2f1* and its non-coding divergently transcribed neighbor *A830082K12Rik* are the only genes significantly upregulated after transient activation of *Nr2f1*, and that *Foxa1* is the only gene significantly upregulated after transient activation of *Foxa1* (Extended Data Fig. 12). These results exclude a role for a network of *trans*-acting factors in enforcing the epigenetic memory of activation observed for these genes. They do not, however, rule out the possibility that the Nr2f1 and Foxa1 TFs themselves trigger direct self-regulating positive feedbacks that are required for inheritance of their respective expression states. In order to test this idea, we introduced a short deletion in *Nr2f1* and short indels in *Foxa1* that are expected to create premature stop codons while minimally altering the transcriptional environment of these genes. We confirmed that no Nr2f1 or Foxa1 protein could be detected after mutation of the corresponding gene even under dCas9-VPR-mediated induction conditions (Fig. 5b). Nevertheless, transient activation of these loci resulted in a persistent memory of expression of their mRNAs at levels on a par with those achieved by deleting *Ezh2* (Fig. 5b). These results strongly suggest that epigenetic memory of active transcription for *Nr2f1* and *Foxa1* is governed in *cis*, independently of the proteins they encode and of other changes in gene expression.

A functional demonstration of true *cis*-acting epigenetic inheritance entails gathering active and inactive alleles within the same nucleus and verifying that the two distinct states are continuously maintained [1,17]. To that end, we fused cells in which we had stably de-repressed wild-type *Nr2f1* or *Foxa1* through transient dCas9-VPR-mediated activation with cells in which the corresponding locus was in its original silent state and carried the mutations depicted in Fig. 5b in order to enable discrimination of the alleles based on their initial expression status (Fig. 5c). After isolating clones of fused cells and confirming their increased ploidy and mononucleated structure (Fig. 5d,e), we performed next-generation sequencing of cDNA to evaluate the respective expression

states of the wild-type, initially active and mutant, initially inactive alleles. We detected the wild-type sequences almost exclusively, indicating that the two expression states had been maintained discretely throughout the many cell divisions required to isolate heterokaryon clones and that any Nr2f1 or Foxa1 protein expressed from wild-type alleles was not sufficient to trigger de-repression of the respective silent alleles in *trans* (Fig. 5f). Importantly, transient induction of dCas9-VPR confirmed that the mutant alleles were present and remained subject to *cis*-regulated epigenetic switching (Fig. 5f, note the appearance of mutant reads in VPR ON and washout conditions). We conclude from these data that the inheritance of transcriptional states at the PRC2 target genes *Nr2f1* and *Foxa1* obeys a *cis*-acting logic.

Discussion

The findings reported here demonstrate that the histone modification H3K27me3 not only constrains transcription but also regulates epigenetic memory of transcriptional states in *cis* at the level of individual gene loci in mammalian cells. In principle, it is possible to envision a system of transcriptional memory structured around self-reinforcing feedbacks of TF networks [1,66], in which the role of a histone modifier such as PRC2 is merely to strengthen the memory by jointly regulating the genes that make up these networks. In this study we have shown that single PRC2 target genes are also capable of autonomously recording comparatively brief transcriptional stimuli into heritable memories in the absence of *trans*-acting feedbacks. We propose that the presence of transcriptional memory at a given locus arises from a hysteretic balance between activating TFs and PRC2 activity that enables transient cues, whether activating or repressive, to produce stable conversion events between bistable states (Fig. 6). Polycomb proteins therefore play a central role in orchestrating a chromatin-based inheritance of epigenetic information, but this memory cannot be explained purely by positive feedback of a self-reinforcing histone modification and is thus fully distinct from many of the previously articulated, semi-conservative models of *cis*-acting memory.

Transcriptional memory of Polycomb target genes is dependent on the cellular context, emerging upon differentiation and displaying striking cell-type specificity. Several genes in particular experience dynamic (reversible) versus epigenetic (irreversible) modes of regulation depending on the cell type. A dynamic mode of transcriptional regulation by Polycomb proteins has also been observed in *Drosophila* both during development [67] and in response to a short pulse of transcription of a transgene linked to a Polycomb Response Element [68]. Our observations relate these distinct modes of regulation to the magnitude of the steady-state activating input, epigenetic memory of transcription requiring a higher input capable of effectively opposing Polycomb activity once a switch has occurred, but not so high that the

Polycomb-silenced state is always overwhelmed (Fig. 6). Epigenetic transcriptional memory of Polycomb target genes is thus structurally linked to the *trans*-acting GRN, which determines the nature and strength of activating inputs experienced by individual genes (α in the model of Fig. 3a,b).

Conversely, *cis*-acting transcriptional memory of Polycomb target genes facilitates the establishment of different epigenetic states downstream of a fixed GRN. This enables, for instance, a given cell type to produce a range of stable antero-posterior identities (defined in large part by the set of expressed Hox genes) without requiring any change in the core GRN. That such multiple stable identities are unlikely to be necessary at pluripotent stages of development might explain why the GRN in mESCs does not appear to potentiate transcriptional memory at Polycomb target genes. Importantly, the mode of *cis*-acting memory we have uncovered is expected to exhibit some degree of flexibility as the complement of TFs for a given target gene evolves according to shifts in developmental context. Overall, our findings provide a mechanism by which short-lived signals can give rise to the type of stable and adaptable transcriptional memory that is an essential condition of multicellular development.

References

1. Bonasio, R., Tu, S. & Reinberg, D. Molecular signals of epigenetic states. *Science* **330,** 612–616 (2010).
2. D'Urso, A. & Brickner, J. H. Mechanisms of epigenetic memory. *Trends in Genetics* **30,** 230–236 (2014).
3. Moazed, D. Mechanisms for the inheritance of chromatin States. *Cell* **146,** 510–518 (2011).
4. Pisco, A. O., d'Herouel, A. F., BioRxiv, S. H.2016. Conceptual Confusion: the case of Epigenetics. *biorxiv.org*

5.   Bostick, M. *et al.* UHRF1 plays a role in maintaining DNA methylation in mammalian cells. *Science* **317,** 1760–1764 (2007).

6.   Catania, S. *et al.* Evolutionary Persistence of DNA Methylation for Millions of Years after Ancient Loss of a De Novo Methyltransferase. *Cell* **180,** 263–277.e20 (2020).

7.   Sharif, J. *et al.* The SRA protein Np95 mediates epigenetic inheritance by recruiting Dnmt1 to methylated DNA. *Nature* **450,** 908–912 (2007).

8.   Audergon, P. N. C. B. *et al.* Epigenetics. Restricted epigenetic inheritance of H3K9 methylation. *Science* **348,** 132–135 (2015).

9.   Coleman, R. T. & Struhl, G. Causal role for inheritance of H3K27me3 in maintaining the OFF state of a Drosophila HOX gene. *Science* **356,** (2017).

10.   Kowalik, K. M. *et al.* The Paf1 complex represses small-RNA-mediated epigenetic gene silencing. *Nature* **520,** 248–252 (2015).

11.   Laprell, F., Finkl, K. & Müller, J. Propagation of Polycomb-repressed chromatin requires sequence-specific recruitment to DNA. *Science* **356,** 85–88 (2017).

12.   Ragunathan, K., Jih, G. & Moazed, D. Epigenetics. Epigenetic inheritance uncoupled from sequence-specific recruitment. *Science* **348,** 1258699 (2015).

13.   Wang, X. & Moazed, D. DNA sequence-dependent epigenetic inheritance of gene silencing and histone H3K9 methylation. *Science* **356,** 88–91 (2017).

14.   Yu, R., Wang, X. & Moazed, D. Epigenetic inheritance mediated by coupling of RNAi and histone H3K9 methylation. *Nature* **558,** 615–619 (2018).

15.   Kuroda, M. I., Kang, H., De, S. & Kassis, J. A. Dynamic Competition of Polycomb and Trithorax in Transcriptional Programming. *Annu. Rev. Biochem.* **89,** 235–253 (2020).

16.   Steffen, P. A. & Ringrose, L. What are memories made of? How Polycomb and Trithorax proteins mediate epigenetic memory. *Nat Rev Mol Cell Biol* **15,** 340–356 (2014).

17.   Berry, S., Hartley, M., Olsson, T. S. G., Dean, C. & Howard, M. Local chromatin environment of a Polycomb target gene instructs its own epigenetic inheritance. *Elife* **4,** 105 (2015).

18.   Beuchle, D., Struhl, G. & Müller, J. Polycomb group proteins and heritable silencing of Drosophila Hox genes. *Development* **128,** 993–1004 (2001).

19.   Jones, R. S. & Gelbart, W. M. Genetic analysis of the enhancer of zeste locus and its role in gene regulation in Drosophila melanogaster. *Genetics* **126,** 185–199 (1990).

20.   Simon, J., Chiang, A. & Bender, W. Ten different Polycomb group genes are required for spatial control of the abdA and AbdB homeotic products. *Development* **114,** 493–505 (1992).

21.   Struhl, G. & Akam, M. Altered distributions of Ultrabithorax transcripts in extra sex combs mutant embryos of Drosophila. *EMBO J* **4,** 3259–3264 (1985).

22.   Reverón-Gómez, N. *et al.* Accurate Recycling of Parental Histones Reproduces the Histone Modification Landscape during DNA Replication. *Molecular Cell* **72,** 239–249.e5 (2018).

23.   Margueron, R. *et al.* Role of the polycomb protein EED in the propagation of repressive histone marks. *Nature* **461,** 762–767 (2009).

24.   Xu, C. *et al.* Binding of different histone marks differentially regulates the activity and specificity of polycomb repressive complex 2 (PRC2). *Proc Natl Acad Sci USA* **107,** 19266–19271 (2010).

25.   Gaydos, L. J., Wang, W. & Strome, S. Gene repression. H3K27me and PRC2 transmit a memory of repression across generations and during development. *Science* **345,** 1515–1518 (2014).

26. Højfeldt, J. W. *et al.* Accurate H3K27 methylation can be established de novo by SUZ12-directed PRC2. *Nat Struct Mol Biol* **20,** 1123–232 (2018).

27. Lavarone, E., Barbieri, C. M. & Pasini, D. Dissecting the role of H3K27 acety-lation and methylation in PRC2 mediated control of cellular identity. *Nature Communications* **10,** 1679 (2019).

28. Oksuz, O. *et al.* Capturing the Onset of PRC2-Mediated Repressive Domain Formation. *Molecular Cell* **70,** 1149–1162.e5 (2018).

29. Sarma, K., Margueron, R., Ivanov, A., Pirrotta, V. & Reinberg, D. Ezh2 re-quires PHF1 to efficiently catalyze H3 lysine 27 trimethylation in vivo. *Mol Cell Biol* **28,** 2718–2731 (2008).

30. He, Y. *et al.* The EED protein-protein interaction inhibitor A-395 inactivates the PRC2 complex. *Nature Chemical Biology* **13,** 389–395 (2017).

31. Konze, K. D. *et al.* An orally bioavailable chemical probe of the Lysine Me-thyltransferases EZH2 and EZH1. *ACS Chem Biol* **8,** 1324–1334 (2013).

32. Ezhkova, E. *et al.* Ezh2 orchestrates gene expression for the stepwise differ-entiation of tissue-specific stem cells. *Cell* **136,** 1122–1135 (2009).

33. Ezhkova, E. *et al.* EZH1 and EZH2 cogovern histone H3K27 trimethylation and are essential for hair follicle homeostasis and wound repair. *Genes Dev* **25,** 485–498 (2011).

34. Wassef, M. *et al.* Impaired PRC2 activity promotes transcriptional instability and favors breast tumorigenesis. *Genes Dev* **29,** 2547–2562 (2015).

35. Woodhouse, S., Pugazhendhi, D., Brien, P. & Pell, J. M. Ezh2 maintains a key phase of muscle satellite cell expansion but does not regulate terminal dif-ferentiation. *J Cell Sci* **126,** 565–579 (2013).

36. Xu, J. *et al.* Landscape of monoallelic DNA accessibility in mouse embryonic stem cells and neural progenitor cells. *Nat Genet* **49,** 377–386 (2017).

37. Chang, H. Y. *et al.* Diversity, topographic differentiation, and positional memory in human fibroblasts. *Proc Natl Acad Sci USA* **99,** 12877–12882 (2002).

38. Baubec, T. *et al.* Genomic profiling of DNA methyltransferases reveals a role for DNMT3B in genic methylation. *Nature* **520,** 243–247 (2015).

39. Morselli, M. *et al.* In vivo targeting of de novo DNA methylation by histone modifications in yeast and mouse. *Elife* **4,** e06205 (2015).

40. Hosogane, M., Funayama, R., Shirota, M. & Nakayama, K. Lack of Transcrip-tion Triggers H3K27me3 Accumulation in the Gene Body. *CellReports* **16,** 696–706 (2016).

41. Riising, E. M. *et al.* Gene silencing triggers polycomb repressive complex 2 recruitment to CpG islands genome wide. *Molecular Cell* **55,** 347–360 (2014).

42. Chen, S. *et al.* The histone H3 Lys 27 demethylase JMJD3 regulates gene expression by impacting transcriptional elongation. *Genes Dev* **26,** 1364–1375 (2012).

43. Lee, M. G. *et al.* Demethylation of H3K27 regulates polycomb recruitment and H2A ubiquitination. *Science* **318,** 447–450 (2007).

44. Pasini, D. *et al.* Characterization of an antagonistic switch between histone H3 lysine 27 methylation and acetylation in the transcriptional regulation of Polycomb group target genes. *Nucleic Acids Res* **38,** 4958–4969 (2010).

45. Tie, F. *et al.* CBP-mediated acetylation of histone H3 lysine 27 antagonizes Drosophila Polycomb silencing. *Development* **136,** 3131–3141 (2009).

46. Deaton, A. M. *et al.* Enhancer regions show high histone H3.3 turnover that changes during differentiation. *Elife* **5,** e1002358 (2016).

47. Kraushaar, D. C. *et al.* Genome-wide incorporation dynamics reveal distinct categories of turnover for the histone variant H3.3. *Genome Biol* **14,** R121 (2013).

48. Beltran, M. *et al.* G-tract RNA removes Polycomb repressive complex 2 from genes. *Nat Struct Mol Biol* **26,** 899–909 (2019).

49. Beltran, M. *et al.* The interaction of PRC2 with RNA or chromatin is mutually antagonistic. *Genome Research* **26,** 896–907 (2016).

50. Schmitges, F. W. *et al.* Histone methylation by PRC2 is inhibited by active chromatin marks. *Molecular Cell* **42,** 330–341 (2011).

51. Yuan, W. *et al.* H3K36 methylation antagonizes PRC2-mediated H3K27 methylation. *Journal of Biological Chemistry* **286,** 7983–7989 (2011).

52. Berry, S., Dean, C. & Howard, M. Slow Chromatin Dynamics Allow Polycomb Target Genes to Filter Fluctuations in Transcription Factor Activity. *Cell Syst* **4,** 445–457.e8 (2017).

53. Lövkvist, C. & Howard, M. Using computational modelling to reveal mechanisms of epigenetic Polycomb control. *Biochem Soc Trans* **49,** 71–77 (2021).

54. Jermann, P., Hoerner, L., Burger, L. & Schübeler, D. Short sequences can efficiently recruit histone H3 lysine 27 trimethylation in the absence of enhancer activity and DNA methylation. *Proc Natl Acad Sci USA* **111,** E3415–21 (2014).

55. Li, H. *et al.* Polycomb-like proteins link the PRC2 complex to CpG islands. *Nature* **549,** 287–291 (2017).

56. Mendenhall, E. M. *et al.* GC-rich sequence elements recruit PRC2 in mammalian ES cells. *PLoS Genet* **6,** e1001244 (2010).

57. Chavez, A. *et al.* Highly efficient Cas9-mediated transcriptional programming. *Nat Meth* **12,** 326–328 (2015).

58. Banaszynski, L. A., Chen, L.-C., Maynard-Smith, L. A., Ooi, A. G. L. & Wandless, T. J. A rapid, reversible, and tunable method to regulate protein function in living cells using synthetic small molecules. *Cell* **126,** 995–1004 (2006).

59. Senturk, S. *et al.* Rapid and tunable method to temporally control gene editing based on conditional Cas9 stabilization. *Nature Communications* **8,** 14370 (2017).

60. Deng, C. *et al.* HoxBlinc RNA Recruits Set1/MLL Complexes to Activate Hox Gene Expression Patterns and Mesoderm Lineage Development. *CellReports* **14,** 103–114 (2016).

61. Hu, M. *et al.* Histone H3 lysine 36 methyltransferase Hypb/Setd2 is required for embryonic vascular remodeling. *Proceedings of the National Academy of Sciences* **107,** 2956–2961 (2010).

62. Xu, Q. *et al.* SETD2 regulates the maternal epigenome, genomic imprinting and embryonic development. *Nat Genet* **51,** 844–856 (2019).

63. Agger, K. *et al.* UTX and JMJD3 are histone H3K27 demethylases involved in HOX gene regulation and development. *Nature* **449,** 731–734 (2007).

64. De Santa, F. *et al.* The histone H3 lysine-27 demethylase Jmjd3 links inflammation to inhibition of polycomb-mediated gene silencing. *Cell* **130,** 1083–1094 (2007).

65. Lan, F. *et al.* A histone H3 lysine 27 demethylase regulates animal posterior development. *Nature* **449,** 689–694 (2007).

66. Ptashne, M. On the use of the word 'epigenetic'. *Curr Biol* **17,** R233–6 (2007).

67. Oktaba, K. *et al.* Dynamic regulation by polycomb group protein complexes controls pattern formation and the cell cycle in Drosophila. *Dev Cell* **15,** 877–889 (2008).

68. Erokhin, M. *et al.* Transcriptional read-through is not sufficient to induce an epigenetic switch in the silencing activity of Polycomb response elements. *Proceedings of the National Academy of Sciences* **112,** 14930–14935 (2015).

Acknowledgments

Author contributions

D.H. and M.W. contributed equally and are listed in alphabetical order. M.W. made the initial observation that certain target genes remained stably de-repressed after transient disruption of PRC2. D.H, M.W. and R.M. conceived the study and designed the experiments with input from all the authors. D.H. and M.W. performed the majority of the experiments. C.L. and M.H. designed, and C.L. performed, all the mathematical modeling. D.Z. performed the bioinformatic analysis. S.A. performed experiments. B.L. carried out the MS experimental work and D.L. supervised MS and data analysis. T.H. assisted in the generation of cell lines. R.M. supervised the study. D.H., M.W. and R.M. prepared the manuscript with input from all the authors.

Competing interests

The authors declare no competing financial interests.

SUPPLEMENTARY INFORMATION

A *cis*-acting mechanism mediates transcriptional memory at Polycomb target genes in mammals

Daniel Holoch[1,2,7], Michel Wassef[1,2,7], Cecilia Lövkvist[3,4*], Dina Zielinski[1,2,5], Setareh Aflaki[1,2], Bérangère Lombard[1,6], Tiphaine Héry[1,2], Damarys Loew[1,6], Martin Howard[3] & Raphaël Margueron[1,2*]

Extended Data Figures 1 to 12

Extended Data Tables 1, 3, 4

Methods

Data availability

Code availability

[1] Institut Curie, Paris Sciences et Lettres Research University, Sorbonne University, 75005 Paris, France. [2] INSERM U934/CNRS UMR 3215, 75005 Paris, France. [3] John Innes Centre, Norwich Research Park, Norwich NR4 7UH, United Kingdom. [4] Present address: Biotech Research and Innovation Centre, University of Copenhagen, 2200 Copenhagen N, Denmark, [5] INSERM U900, Mines ParisTech, 75005 Paris, France. [6] Proteomics Mass Spectrometry Laboratory, 75005 Paris, France. [7] These authors contributed equally: Daniel Holoch, Michel Wassef. *e-mail: cecilia.loevkvist@bric.ku.dk, raphael.margueron@curie.fr.

Extended Data Table 1. Quantification of histone marks.

Peptide sequence and modification position	Protein modification (without N-term. Met)	Mock	PRC2i	Adj. p-value	CV %
K[Ac]SAPATGGVK	Acetyl (K27)	1.55×10^8	2.14×10^8	0.2365	71.8713
K[Ac]SAPATGGVKKPHR	Acetyl (K27)	4.29×10^5	1.58×10^6	0.2017	62.9365
K[Ac]SAPATGGVK[me]KPHR	**Acetyl (K27), Methyl (K36)**	**7.88×10^6**	**2.67×10^7**	**0.0099**	**20.2150**
K[Ac]SAPATGGVK[Dime]KPHR	**Acetyl (K27), Dimethyl (K36)**	**1.43×10^7**	**5.93×10^7**	**0.0252**	**27.3137**
K[me]SAPATGGVK	**Methyl (K27)**	**5.28×10^8**	**1.67×10^8**	**0.0002**	**6.6260**
K[me]SAPATGGVK[me]KPHR	**Methyl (K27), Methyl (K36)**	**6.73×10^7**	**2.27×10^7**	**0.0025**	**13.4713**
K[me]SAPATGGVK[Dime]KPHR	**Methyl (K27), Dimethyl (K36)**	**1.53×10^8**	**4.63×10^7**	**0.0019**	**11.9292**
K[Dime]SAPATGGVK	**Dimethyl (K27)**	**1.34×10^9**	**5.11×10^7**	**0.0000**	**2.0606**
K[Dime]SAPATGGVK[me]KPHR	**Dimethyl (K27), Methyl (K36)**	**1.68×10^8**	**1.46×10^7**	**0.0001**	**5.4057**
K[Dime]SAPATGGVK[Dime]KPHR	**Dimethyl (K27), Dimethyl (K36)**	**2.17×10^8**	**4.68×10^6**	**0.0001**	**4.6181**
K[Trime]SAPATGGVK	**Trimethyl (K27)**	**3.44×10^8**	**1.38×10^6**	**0.0001**	**3.7323**
K[TriMe]SAPATGGVK[me]KPHR	**Trimethyl (K27), Methyl (K36)**	**8.71×10^7**	**2.13×10^6**	**0.0001**	**4.8148**
K[Trime]SAPATGGV[Dime]KKPHR	**Trimethyl (K27), Dimethyl (K36)**	**3.25×10^7**	**4.15×10^5**	**0.0001**	**5.6788**

Peptide abundances represent peak areas normalized to those of the peptide STELLIR (residues 57-63) in arbitrary units without logarithmic transformation. Peptide abundances with a p-value < 0.05 were considered to be significantly altered in PRC2i samples and are indicated in bold.

Extended Data Table 3. Sequences of primers used for quantitative PCR.

Description	Sequence
Drosophila S2 Ubx, CUT&RUN forward [69]	TCCAATCCGTTGCCATCGAACGAAT
Drosophila S2 Ubx, CUT&RUN reverse [69]	TTAGGCCGAGTCGAGTGAGTTGAGT
Nr2f1, CUT&RUN forward	ACCCTGCTTTCATAGTAGTGTCATT
Nr2f1, CUT&RUN reverse	TATTTAAGCAGAGGGTGGAGTTTGA
Foxa1, CUT&RUN forward	CTTGGGAATTTTAAGTTGGTCCGAA
Foxa1, CUT&RUN reverse	TCTGTTACCTGTTTGTAGTCCTCTG
Tbp, RT-qPCR forward	ATCCCAAGCGATTTGCTG
Tbp, RT-qPCR reverse	CCTGTGCACACCATTTTTCC
Alx1, RT-qPCR forward	AAAGCGACGGCTGGCAAATGCG
Alx1, RT-qPCR reverse	ATTCAGCTCGGTGTGAAGGGGC
Nr2f1, RT-qPCR forward	CTTAACTTACACATGCCGTGCC
Nr2f1, RT-qPCR reverse	GAGGCATTCTTCCTCGCTGAAC
Foxa1, RT-qPCR forward	AACAGCTACTACGCGGACACGC
Foxa1, RT-qPCR reverse	ATGTTGCCGCTCGTGGTCATGG
Hoxb13, RT-qPCR forward	AAACGCTTAGGATTCCCTGGGCCT
Hoxb13, RT-qPCR reverse	AAGGTGGCATAATTGCCGGGCT
Hoxb6, RT-qPCR forward	ACAGGACAAGAGCGTGTTCGGA
Hoxb6, RT-qPCR reverse	GCCCAAAAGAGGAACTGTTGCACG
Hoxb9, RT-qPCR forward	TCAAAGAGCTGGCTACGGGGACAA
Hoxb9, RT-qPCR reverse	GCTCCAGCGTCTGGTATTTGGTGT
lncRNA-Hoxb, RT-qPCR forward	TCCCGTGCCTTGTTGCCTTGAT
lncRNA-Hoxb, RT-qPCR reverse	TGGTGGAGGTGGTGGGGCATAAAA
Hoxb5, RT-qPCR forward	ACATCAGCCACGATATGACTGGGC
Hoxb5, RT-qPCR reverse	GGGTCAGGTAGCGATTGAAGTGGA

Extended Data Table 4. Sequences encoding gRNAs.

Description	Sequence
Setd2 deletion gRNA 1	GTCGGTCCGAAAGAGATCGA
Setd2 deletion gRNA 2	AGCGTGTCCTCTCACGATAA
Utx deletion gRNA 1	GGTAGCGAGCGACACTCCGC
Utx deletion gRNA 2	ATGGCGGCGGGAAAAGCGAG
Jmjd3 deletion gRNA 1	TCGGGCAGTGGACCCTCCAG
Jmjd3 deletion gRNA 2	CGAAGCTCATGGCTGCCCGG
Crebbp deletion gRNA	GCCAGCAGCCCTGTGCAACA
Nr2f1 deletion gRNA 1	CCAGTATGCACTCACAAACG
Nr2f1 deletion gRNA 2	GCAGAGAAATGTAGCCAGAC
Foxa1 mutation gRNA	CATGGTGTTCATGGTCATGT
Alx1 activation gRNA 1	GCGGGGACGCGCCCTACCCT
Alx1 activation gRNA 2	GGCCCTACCCTGGGTAAGGA
Nr2f1 activation gRNA 1	GTGGTCAGAGCCCTGAATGG
Nr2f1 activation gRNA 2	GCCAACCAATGGCGTGAAGG
Foxa1 activation gRNA 1	GCCGAGGTGCACCTGTGAGG
Foxa1 activation gRNA 2	GTCCCGCAGCACAGCTCTTT
Hoxb13 activation gRNA 1	GCATGAGCGCTGATTGGCTG
Hoxb13 activation gRNA 2	GAGAAATTGCAGGGGGAGAA
Hoxb6 activation gRNA 1	GAGGAGCGCAGCCTGCACGA
Hoxb6 activation gRNA 2	GTGCAGGCTGCGCTCCTCCT
Hoxb9 activation gRNA 1	GTCTCAACATGGGGCGATGG
Hoxb9 activation gRNA 2	GAGCTCAGGCTGAGGTTACG
lncRNA-Hoxb activation gRNA 1	ATTGGCCGGCGCCGGTCATG
lncRNA-Hoxb activation gRNA 2	GAATTTATTGCATTTCTTCA
DD-dCas9-VPR deletion gRNA 1	CTAAAACCGGAACCGGACAA
DD-dCas9-VPR deletion gRNA 1	CGGTATTGTCTCCTTCCGTG

Methods

<u>Plasmids</u>

The MSCVhygro-Flag-Ezh2 retroviral vector was purchased from Addgene (24296).

Plasmids for targeting intron 15 of Ezh2 included (1) a gRNA cloning vector (Addgene 41824, [70]) engineered to express the gRNA sequence 5'-GTTACTATGTTGCCAAGTAG and (2) a targeting vector containing an *En2*-splice-acceptor-T2A-hygroR-SV40polyA cassette flanked by FRT sites [71], further flanked by sequences for homology-directed repair corresponding to the targeted region of Ezh2, cloned from mouse genomic DNA.

PB-TRE-FKBP12DD-dCas9-VPR was generated by inserting the FKBP12-L106P destabilizing domain (DD) [58] into PB-TRE-dCas9-VPR (Addgene 63800, [57]) as an N-terminal fusion domain.

The hyperactive PiggyBac transposase expression vector pCMV-hyPBase[72] was a gift from F. Stewart.

pLKO.1-blast-U6-sgRNA-BfuA1-stuffer was generated by replacing the puromycin resistance gene in pLKO.1-puro-U6-sgRNA-BfuA1-stuffer (Addgene 50920, [73]) with a blasticidin resistance gene. Dual-guide constructs were generated by linearizing the resulting plasmid with BfuA1 and using Gibson assembly to insert a PCR product containing one gRNA sequence, the invariant sgRNA scaffold sequence, a modified murine U6 promoter [74] and a second gRNA sequence. The plasmid backbone provides a human U6 promoter for the first sgRNA (5') and the scaffold sequence for the second sgRNA (3').

pX458 was purchased from Addgene (48138, [75]).

hCas9-without-neo was generated by excising the neomycin resistance gene from hCas9 (Addgene 41815, [70]) with DraIII and BstZ17I.

hCas9-PID-NAA-BPNLS was constructed from hCas9 by replacing the sequence encoding the protospacer-adjacent motif (PAM) interaction domain (PID) with the corresponding sequence from the iSpy Cas9, which recognizes the PAM NAA [76], using a plasmid template that was a gift from J.-P. Concordet, and by replacing the C-terminally-encoded SV40 NLS with a bipartite NLS [77,78].

pCDH-CMV-EF1α-Flag-neo (System Biosciences) was used to confer resistance to G418 via lentiviral transduction.

<u>Cell lines</u>

Mouse neural progenitor cells (NPCs), derived by *in vitro* differentiation [79] of embryonic stem cells isolated from a cross between a 129/Sv female and a Cast/EiJ male, were a gift from A.-V. Gendrel and E. Heard (clone C2, described in [80]). NPCs were grown in gelatin-coated flasks in N2B27 medium (50% DMEM/F-12, 50% neurobasal medium, 2 mM L-glutamine, 1X NDiff Neuro2 supplement (Millipore), 0.5X B27 supplement (Gibco), 0.1 mM 2-mercaptoethanol) supplemented with 10 ng/mL EGF (Peprotech) and 10 ng/mL FGF2 (Peprotech), and passaged using Accutase (Gibco).

Mouse embryonic stem cells (mESCs) ES-E14TG2a (ATCC CRL-1821 lot #62909865) were a kind gift from M. Schulz and D. Bourc'his. mESCs were grown in gelatin-coated flasks in 2i+LIF medium (N2B27 medium described just above, supplemented with 3 µM CT-99021 (Selleck Chemicals), 1 µM PD0325901 (Selleck Chemicals) and 10 ng/mL LIF (Miltenyi Biotec)), and passaged using Accutase (Gibco).

Immortalized mouse embryonic fibroblasts (iMEFs) were grown in DMEM high-glucose supplemented with 10% fetal calf serum, nonessential amino acids and 2 mM L-glutamine. iMEFs were obtained by isolating MEFs from a male *Ezh2^flox/Δ^* ; *Rosa26::Cre-ERT2* 13.5-day-old embryo (iMEF A, [34]) or a female *Ezh2^flox/flox^* ; *Rosa26::Cre-ERT2* 13.5-day-old embryo (iMEF B, [81]), infecting them with pMXs-hc-MYC (Addgene 17220) and deriving a clone via limiting dilution.

Deletion of *Ezh2* in iMEF A was achieved by treatment with 100 nM 4-hydroxytamoxifen (Sigma) and rescue was performed by infection with a MSCVhygro-Flag-Ezh2 ecotropic retrovirus and selection with 0.4 mg/mL hygromycin B. Reversible deletion of *Ezh2* in iMEF B was achieved by homozygous CRISPR-Cas9-mediated integration of an *En2*-splice-acceptor-T2A-hygroR-SV40polyA cassette, flanked by FRT sites [71], into intron 15 of *Ezh2* under selection with 0.4 mg/mL hygromycin B. Genetic rescue of *Ezh2* was performed by transfecting cells with pCAGGS-flpE-puro (Addgene 20733) and screening for clones having undergone homozygous excision of the *En2*-splice-acceptor-T2A-hygroR-SV40polyA cassette.

Inhibition of PRC2
Inhibition of PRC2 activity in NPCs, mESCs and iMEF B was achieved by simultaneous treatment with 2 μM UNC1999 (Sigma) and 4 μM A395 (Sigma).

Differentiation of NPCs to astrocytes
Differentiation of NPCs into astrocytes was performed as previously described [80]. NPCs were plated in 6-well plates and grown for 48 h, then washed twice with N2B27 medium and cultured in N2B27 supplemented with 1 ng/ml FGF2 and 10ng/ml BMP4 (R&D Systems) for 48 h.

Antibodies
Anti-Nestin was a kind gift from V. Ribes; anti-GFAP (Z033429-2) was purchased from Agilent Technologies; anti-H2AK119ub1 (D27C4), anti-H3K4me3 (C42D8), anti-H3K27me3 (C36B11), anti-H4 (L64C1), anti-Hdac1 (10E2) and anti-Crebbp (D6C5) were purchased from Cell Signaling Technology; anti-Pol II (N-20) was purchased from Santa Cruz; anti-H3K27ac (ab4729), anti-H3K36me3 (ab9050), anti-Lamin B1 (ab16048), anti-Nr2f1 (ab181137) and anti-Foxa1 (ab23738) were purchased from Abcam; anti-Utx (A302-374A) was purchased from Bethyl; anti-Jmjd3 was a gift from E. Heard; and anti-Cas9 antibody was a gift from A. El Marjou at the Institut Curie Protein Expression and Purification Core Facility. Alexa Fluor secondary antibodies for immunofluorescent staining were purchased from Invitrogen. StarBright Blue 700 fluorescent secondary antibodies for Western blot were purchased from Bio-Rad.

Immunofluorescent staining
NPCs and astrocytes were cultured on gelatin-coated coverslips before being processed for immunofluorescent staining. Cells were then washed once with PBS, fixed in 4% paraformaldehyde for 5 minutes at room temperature (RT) followed by a wash in PBS. Permeabilization was achieved in PBS containing 0.5% Triton-X 100 for 5 minutes at RT followed by 4 washes in PBS. Cells were then blocked in PBS containing 20 % goat serum for a minimum of 30 minutes at RT, followed by a wash in incubation buffer (0.001 % Tween-20, 0.1 % BSA, 1 mM sodium azide in PBS). Cells were then incubated with primary antibodies diluted in incubation buffer overnight at 4 °C, washed 4 times in PBS, incubated with fluorescently labeled secondary antibodies 1-2 h at RT and washed 3 times in PBS before mounting in DAPI-containing Vectashield mounting medium.

Nuclear extracts for Western blot
Nuclear extracts for Western blot were prepared by incubating cells in buffer A (10 mM HEPES-NaOH pH 7.9, 2.5 mM $MgCl_2$, 0.25 M sucrose, 0.1% NP-40, 1 mM DTT, 1 mM PMSF) for 10 min on ice to lyse, centrifuging at 6000 g for 10 min to pellet nuclei, resuspending nuclei in buffer B (25 mM HEPES-NaOH pH 7.9, 1.5 mM $MgCl_2$, 0.7 M NaCl, 0.1 mM EDTA, 20% glycerol, 1 mM DTT, 1 mM PMSF), sonicating for 3 x 15 s using a Branson Sonifier at 10% amplitude, centrifuging at 20,000 g for 15 min and recovering the supernatant.

Image acquisition
Image acquisition for immunofluorescent staining was performed with an epifluorescence microscope (Leica), using a fluorescence camera (CoolSnap HQ2). Image acquisition for Western blot was performed using a ChemiDoc MP Imaging System (Bio-Rad). Images were further processed with ImageJ software.

Clonal growth assay
Cells, either mock-treated, undergoing continuous PRC2 inhibition, or having previously undergone PRC2 inhibition, were plated at low confluence and then imaged in an Incucyte device by phase contrast at regular intervals.

Propidium iodide staining and FACS analysis
Cells were resuspended in a nuclear-staining solution (1 mg/mL sodium citrate, 100 mM NaCl, 0.1% NP-40, 50 μg/mL RNase A, 25 μg/mL Propidium iodide) and analyzed on a NovoCyte flow cytometer.

Apoptosis assay
Cells, either mock-treated, undergoing continuous PRC2 inhibition, or having previously undergone PRC2 inhibition, were plated in the presence of Incucyte Caspase-3/7 Green Dye for Apoptosis (Essen Biosciences) and, in the case of mock-treated cells, in the presence or absence of 0.5 mM H_2O_2. Cells were imaged in an Incucyte device by phase contrast and green fluorescence after 12 h. Green object count and cell confluence were determined automatically by Incucyte software and results were confirmed by visual inspection of the images.

Quantification of histone modifications by Parallel-Reaction Monitoring
Total histones were extracted from the nuclei of NPCs (mock-treated or treated with the PRC2 inhibitors indicated above) with sulfuric acid as previously described [82]. Three biologically independent histone purifications were simultaneously separated by SDS-PAGE and stained with colloidal blue (LabSafe Gel Blue GBiosciences). One gel slice was excised for each purification and in-gel digested using trypsin/LysC (Promega). Peptides extracted from each band were then analyzed by nanoLC-MS/MS (RSLCnano system coupled to a Q Exactive HF-X). Separation was performed after direct injection on a 50 cm x 75 μm C18 column (nanoViper C18, 3 μm, 100Å, Acclaim PepMapTM RSLC, Thermo Scientific) regulated to 50°C and with a linear gradient from 2% to 35% buffer B at a flow rate of 300 nL/min over 94 min. The mass spectrometer was operated in PRM mode (see acquisition list in Table M1 below). The acquisition list was generated from the peptides obtained from the mix of samples (all 3 replicates) of the mock-treated condition based on the DDA results.

Table M1. Targeted peptides.

Peptide Modified Sequence Full Names	Protein Modification without N-term. Met	Mass [m/z]	Charge	Extracted fragments
K[Ac]SAPATGGVKKPHR	Acetyl (K27)	738.42574	2	y3, y4, y5, y8, y9, y9++, y10, y10++, y11, y11++, y12++, b2, b3, b3, b11
K[Ac]SAPATGGVK[me]KPHR	Acetyl (K27), Methyl (K36)	745.43357	2	y3, y4, y8, y9, y9++, y10, y11, y11++, y12, y12++, y13++, b2, b3, b11
K[Ac]SAPATGGVK[Dime]KPHR	Acetyl (K27), Dimethyl (K36)	752.44139	2	y3, y4, y8, y9, y9++, y10, y11, y11++, y12, y12++, y13++, b2, b3, b11
K[Ac]SAPATGGVK	Acetyl (K27)	479.27187	2	y2, y3, y4, y5, y6, y7, y8, y9, b2, b3
K[me]SAPATGGVK[me]KPHR	Methyl (K27), Methyl (K36)	731.43611	2	y3, y8, y9, y10, y11, y11++, y12, y12++, y13, b1, b3, b11, b13
K[me]SAPATGGVK[Dime]KPHR	Methyl (K27), Dimethyl (K36)	738.44393	2	y3, y8, y9, y10, y11, y11++, y12, y12++, y13, b1, b2, b3, b11, b13
K[me]SAPATGGVK	Methyl (K27)	465.27441	2	y2, y3, y4, y5, y7, y8, y9, b1, b2, b3, b5, b8, b9
K[Dime]SAPATGGVK[me]KPHR	Dimethyl (K27), Methyl (K36)	738.44393	2	y3, y4, y8, y11, y11++, y12, y12++, y13, y13++, b2, b3, b10, b11, b13
K[Dime]SAPATGGVK[Dime]KPHR	Dimethyl (K27), Dimethyl (K36)	745.45176	2	y3, y4, y8, y11, y11++, y12, y12++, y13, y13++, b2, b3, b11, b13, b13++
K[Dime]SAPATGGVK	Dimethyl (K27)	472.28224	2	y2, y3, y4, y5, y7, y7++, y8, y9, b5, b7, b7++, b8, b8++
K[TriMe]SAPATGGVK[me]KPHR	Trimethyl (K27), Methyl (K36)	745.45176	2	y3, y4, y8, y9, y11, y12++, y13, y13++, b10, b11, b11++, b13, b13++
K[Trime]SAPATGGV[Dime]KKPHR	Trimethyl (K27), Dimethyl (K36)	752.45958	2	y3, y4, y8, y9, y10, y11, y11++, y12++, y13, y13++, b11, b13, b13++
K[Trime]SAPATGGVK	Trimethyl (K27)	479.29006	2	y2, y3, y4, y7, y7++, y8, y9, b3, b5, b8, b9
STELLIR		416.2504	2	y2, y3, y3++, y4, y5, y6, b2, b3

PRM Data Analysis

The PRM data were analyzed using Skyline version (version 20.1.0.155) MacCoss Lab Software, Seattle, WA; (https://skyline.ms/project/home/software/Skyline/begin.view), fragment ions for each targeted mass (Table M1) were extracted and peak areas were integrated. Data analysis was then performed using myProMS (v3.9.1, [83]). For each peptide, the mean

peak areas were normalized by the STELLIR peptide fragment mean area. On each peptide, a linear model was applied to compute a regression coefficient between the conditions (used as fold change) and its associated p-value. The p-values were corrected for multiple testing using the Benjamini-Hochberg procedure.

CUT&RUN and CUT&RUN-seq

CUT&RUN was performed as described [84], starting from a mixture of 500,000 mouse cells and 25,000 *Drosophila melanogaster* Schneider 2 cells (grown in Schneider's medium supplemented with 10% heat-inactivated fetal calf serum) for CUT&RUN-seq, or 500,000 mouse cells and 100,000 *Drosophila* S2 cells for CUT&RUN for quantitative PCR (qPCR) analysis. Eluted DNA was purified using the NucleoSpin kit (Macherey-Nagel) according to the manufacturer's instructions. Primer sequences used for qPCR analysis are listed in Extended Data Table 3 (normalization was performed using the *Drosophila Ubx* locus).

For CUT&RUN-seq, libraries were prepared using the Accel-NGS 2S Plus DNA library kit (Swift Biosciences) according to the manufacturer's instructions, and sequenced on an Illumina Novaseq 6000 (PE100) at the Institut Curie Next Generation Sequencing Core Facility. Reads were simultaneously mapped to the *Mus musculus* (GRCm38/mm10) and *Drosophila melanogaster* (dm6) genomes with Bowtie 2 (2.2.9) using end-to-end alignment (very-sensitive). PCR duplicates were removed with Picard Tools MarkDuplicates (1.97) and mm10/dm6 reads were split into separate BAM files. Reads mapping to the *Drosophila* genome were counted into 10kb bins and scale factors were calculated using the median ratio method implemented in DESeq2 estimateSizeFactors (1.22.2). Properly paired reads mapping to the mouse genome were counted once in bins of length 50. RPKM per bin were multiplied by the scale factor and converted to bigWig format using DeepTools bamCoverage. *Mus musculus* BAM files were filtered to exclude common artifact regions: https://github.com/Boyle-Lab/Blacklist/tree/master/lists and only autosomes and reads with MAPQ>10 were retained for the analysis.

ChIP-seq

Cell confluence and starting material were kept constant by plating a defined number of cells in 15-cm dishes two days before cross-linking. Cells were cross-linked in the culture dishes by incubating at room temperature for 10 min in cross-linking medium (DMEM supplemented with 15 mM HEPES-NaOH pH 7.9, 15 mM NaCl, 0.15 mM EDTA, 0.075 mM EGTA and 1% formaldehyde) pre-warmed to 37°, followed by quenching with 0.125 M glycine at room temperature for 5 min. Cells were then rinsed with cold PBS, scraped from the dishes in PBS and transferred to 15-mL conical tubes, pelleted and washed again in PBS. Next, cells were lysed by incubation at 4° for 10 min in 1 mL buffer 1 (50 mM HEPES-KOH pH 7.5, 140 mM NaCl, 1 mM EDTA, 10% glycerol, 0.5% NP-40, 0.25% Triton X-100 supplemented with 1 µM pepstatin A, 10 µg/mL aprotinin, 1 µg/mL leupeptin and 1 mM PMSF). Nuclei were pelleted, resuspended in 1 mL buffer 2 (10 mM Tris-HCl pH 8, 200 mM NaCl, 1 mM EDTA, 0.5 mM EGTA supplemented with 1 µM pepstatin A, 10 µg/mL aprotinin, 1 µg/mL leupeptin and 1 mM PMSF) and incubated at room temperature for 10 min. Nuclei were pelleted again, resuspended in 1.3 mL buffer 3 (10 mM Tris-HCl pH 8, 1 mM EDTA, 0.5 mM EGTA, 0.5% N-lauroyl-sarcosine supplemented with 1 µM pepstatin A, 10 µg/mL aprotinin, 1 µg/mL leupeptin and 1 mM PMSF) and sonicated using a Diagenode Bioruptor cooled to 4°, for 30 x 30 s with 30-s pauses. Solubilized chromatin was then recovered by centrifuging at 20,000 *g* and saving the supernatant. Chromatin concentrations were estimated by Bradford assay and then equalized using buffer 3.

Protein A Dynabeads (Invitrogen), 10 µL slurry per chromatin sample, were washed three times in 100 µL 0.5% BSA in PBS per sample and incubated on rotator for

several hours during chromatin preparation in 40 µL 0.5% BSA in PBS per sample and 2.5 µL antibody per sample.

Just prior to beginning the immunoprecipitation, 0.5 volume buffer 4 (15 mM EDTA, 3% Triton X-100, 0.3% sodium deoxycholate supplemented with 3 µM pepstatin A, 30 µg/mL aprotinin, 3 µg/mL leupeptin and 3 mM PMSF) was added to each chromatin sample, and one-tenth the resulting volume was set aside as input. Dynabeads were washed three more times in 100 µL 0.5% BSA in PBS per chromatin sample, resuspended in 10 µL of a 2:1 mixture of buffers 3 and 4 per sample and distributed 10 µL to each sample for the immunoprecipitation, carried out at 4° overnight on rotator.

After immunoprecipitation, beads were washed six times in 0.4 mL ice-cold buffer 5 (50 mM HEPES-KOH pH 7.5, 0.5 M LiCl, 10 mM EDTA, 0.7% sodium deoxycholate, 1% NP-40 supplemented with 1 µM pepstatin A, 10 µg/mL aprotinin, 1 µg/mL leupeptin and 1 mM PMSF) with 2 min room-temperature rotation per wash, and once in 0.4 mL 10 mM Tris-HCl pH 8, 50 mM NaCl, 1 mM EDTA. Precipitated chromatin was then eluted by incubating beads in 200 µL 50 mM Tris-HCl, 10 mM EDTA, 1% SDS with shaking at 65° for 30 min. Eluted chromatin, and input samples brought to 200 µL with 50 mM Tris-HCl, 10 mM EDTA, 1% SDS, were incubated overnight at 65° to reverse cross-links, and then treated with 80 µg RNase A at 37° for 1 h and 40 µg proteinase K at 55° for 1 h. DNA was extracted with phenol:chloroform:isoamyl alcohol and precipitated in ethanol.

Libraries were prepared by the Institut Curie Next Generation Sequencing Core Facility using the TruSeq ChIP sample preparation kit (Illumina) according to the manufacturer's instructions and sequenced on an Illumina HiSeq 2500 (PE50 for H3K27me3, SE50 for Pol II, H3K4me3, H3K36me3 and H2AK119ub1). ChIPseq libraries were aligned to mm10 using Bowtie 2 (2.2.9) with default parameters. PCR duplicates were removed with Picard Tools MarkDuplicates (1.97) and BAM files were filtered to exclude common artifact regions: https://github.com/Boyle-Lab/Blacklist/tree/master/lists and only reads covering autosomes with MAPQ>10 were retained for the analysis. Reads were counted over gene body coordinates (obtained from the gencode vM13 GTF) with FeatureCounts, allowing reads to overlap all meta-features.

CUT&RUN-seq and ChIP-seq peak calling
H3K27me3 peaks were called in NPC and iMEF samples with the respective PRC2-disrupted sample as control using MACS2 (2.1.1.20160309) on combined replicates with the following parameters: -f BAMPE --gsize mm --broad --broad-cutoff 0.1 --bdg.

Analysis of published mESC ChIP-seq data
FASTQ files from ChIP-sequencing of WT and Ezh1/Ezh2 dKO murine ESCs from GEO Series GSE103685 (SRR6025332, SRR6025341) were downloaded from the EBI European Nucleotide Archive.

Mapping, filtering and peak calling were performed as for NPCs and iMEFs.

RNA-seq
Total RNA was isolated by Trizol extraction. Libraries were prepared either by the Institut Curie Next Generation Sequencing Core Facility using the Illumina TruSeq Stranded mRNA kit (NPCs) or TruSeq Stranded Total RNA kit according to the manufacturer's instructions (all iMEF samples except those shown in Extended Data Fig. 3f), or using the Swift RNA Library kit (Swift Biosciences) (mESCs, iMEFs in Extended Data Fig. 3f), and sequenced on an Illumina Novaseq 6000 (PE100, NPCs, mESCs, and iMEFs in Extended Data Figs. 3f and 12a) or HiSeq 2500 (PE50, all other iMEFs).

Chromatin-associated nascent RNA was isolated from 20 million cells by a procedure kindly shared by M.A. Maqbool and J.-C. Andrau. After resuspension and

incubation in 4 mL HLB/NP40 buffer (10 mM Tris-HCl pH 7.5, 10 mM NaCl, 2.5 mM MgCl$_2$, 0.5% NP-40) for 5 min on ice, 1 mL HLB/NP-40 buffer also containing 10% sucrose was underlain and nuclei were collected by centrifugation for 5 min at 1400 g. Nuclei were resuspended in 125 μL NUN1 buffer (20 mM Tris-HCl pH 8.0, 75 mM NaCl, 0.5 mM EDTA, 50% glycerol supplemented with 1 μM pepstatin A, 10 μg/mL aprotinin, 1 μg/mL leupeptin and 1 mM PMSF), followed by 1.2 mL NUN2 buffer (20 mM HEPES-KOH pH 7.6, 7.5 mM MgCl$_2$, 0.2 mM EDTA, 300 mM NaCl, 1 M urea, 1% NP-40, supplemented with 1 μM pepstatin A, 10 μg/mL aprotinin, 1 μg/mL leupeptin and 1 mM PMSF), and then incubated on ice for 15 minutes with 5 s vortexing every 4 min. A 10 min centrifugation at 15,000 g separated the nucleoplasm supernatant, which was not further processed, from the chromatin pellet, which was washed in 0.5 mL NUN2 buffer and collected again by centrifugation for 10 min at 15,000 g. Trizol extraction from the chromatin pellet, with brief incubations at 95° as necessary to fully dissolve the material, yielded the nascent RNA, which was then subjected to library preparation and sequencing as above (TruSeq Stranded Total RNA kit, HiSeq 2500, PE50).

Libraries are strand-specific (reverse) according to RSeQC (2.6.4) after sampling 200,000 reads with MAPQ>30. Raw reads were trimmed for adapters with Cutadapt (1.12) using the Trim Galore! (0.4.4) wrapper (default settings) and subsequently mapped to the complete mouse rRNA sequence with Bowtie 2 (2.2.9). Reads that failed to align to rRNA were mapped with TopHat2 (2.1.1)/Bowtie 2 (2.2.9) to mm10 and gene counts by gene or exons were generated using FeatureCounts (1.5.1). Reads were assigned to all overlapping features (exon or gene) in order to count those that fall completely within another gene (e.g., *Hoxb6*).

Differential expression analysis of H3K27me3-positive genes

Differential expression (DE) analysis was performed comparing the different biological conditions separately for each cell line using the edgeR glmFit (negative binomial generalized linear model with likelihood ratio tests). Genes with counts per million (CPM) > 0.5 in at least 2 samples whose transcription start site (TSS)+3kb overlapped an H3K27me3 peak (minimum 1bp overlap) were categorized as H3K27me3-positive. Library sizes were scaled using the trimmed mean of M values (TMM) method and dispersion was estimated by weighted likelihood empirical Bayes.

A negative binomial generalized log-linear model was fit to the read counts for each gene. Differentially expressed genes for each comparison were identified from the linear fit after adjusting for multiple testing and filtered to include those with false-discovery-rate- (FDR-) -adjusted p-value < 0.05 and absolute log2FoldChange > 1.

Among genes categorized as H3K27me3-positive, those significantly upregulated in PRC2-disrupted v. WT/mock are considered PRC2-responsive. Among PRC2-responsive genes, those significantly upregulated in PRC2-rescue v. WT/mock but not upregulated in PRC2-disrupted v. PRC2-rescue are considered irreversible, while those significantly upregulated in PRC2-disrupted v. PRC2-rescue but not in PRC2-rescue v. WT/mock are considered reversible; all other PRC2-responsive genes are considered intermediate. Intermediate genes are included in the totals represented in Extended Data Fig. 3a,b but excluded from the totals represented in Fig. 1f.

Gene expression heatmaps were generated using TreeView [85].

Analysis of published NPC and mESC RNA-seq data

FASTQ files from RNA sequencing of murine NPCs and ESCs from GEO Series GSE54016 (SRR1106775 through SRR1106784) were downloaded from the EBI European Nucleotide Archive.

Mapping and assignment to exons were performed as above.

Principal component analysis was carried out using R (3.6.1), and the varcontrib output was used to compute arithmetic differences in percent contribution

of each gene to dimensions 1 and 2 (the latter capturing experimental batch effects) in order to select genes for the heat map in Extended Data Fig. 2b.

Read count normalization

Read counts over gene body (RNA-seq and ChIP-seq/CUT&RUN) were normalized by gene length (kb) and library size (TMM normalization factors were calculated using edgeR) as follows:

$$\left(\sum_{i}^{n} \frac{counts_i}{length_i} * TMM_{norm} \right) / 10^6$$

Analysis of published NPC ATAC-seq data

FASTQ files from ATAC-seq of NPC clone XX_2 from GEO Series GSE84646 (SRR3933589, SRR3933585 and SRR3933586) were downloaded from the EBI European Nucleotide Archive. Reads were aligned to mm10 using Bowtie 2 (2.2.9) allowing an insert size of up to 2 kb with the following parameters: '--reorder -p 8 -D 70 -R 3 -N 0 -L 20 -i S,1,0.50 -X 2000'. BAM files were filtered to exclude reads mapping to mitochondria or common artifact regions (http://mitra.stanford.edu/kundaje/akundaje/release/blacklists/mm10-mouse/mm10.blacklist.bed.gz).

ATAC-seq on iMEF A cells

ATAC-seq was performed as previously described [86] with transposition on 50,000 whole cells rather than nuclei in order to minimize mitochondrial DNA contamination as recommended by [87]. Libraries were sequenced on an Illumina HiSeq 2500 (PE100). Mapping and filtering were performed as for NPCs.

ATAC-seq peak calling and differential enrichment analysis

Peak calling on ATAC-seq in iMEF A was performed on each replicate using SEACR [88] with a threshold of 0.006 and "stringent" mode, and Intersect (Galaxy v1.0.0) was used to identify overlapping pieces of intervals. Differential enrichment analysis on iMEF A Ezh2 KO peaks was done with EdgeR with the likelihood ratio test. Differentially enriched peaks for each comparison were identified after adjusting for multiple testing and filtered to include those with false-discovery-rate (FDR)-adjusted p-value < 0.05 and positive log2 fold change.

Gene ontology term enrichment analysis

For each gene set analyzed, significantly enriched biological process gene ontology (GO) terms were retrieved using Gorilla [89]. The top 100 most significantly enriched GO terms (with FDR-adjusted p-value < 0.05) were further processed by Revigo [90] in order to remove redundant GO terms. Only the top 10 are reported.

Motif enrichment analysis

Enrichment of known motifs was determined using HOMER v. 4.7 [91] and the most recently available list of motif position-weight matrices provided on the HOMER website (http://homer.ucsd.edu/homer/custom.motifs). Clustering of transcription factor binding motifs was carried out using RSAT [92].

Whole-Genome Bisulfite Sequencing (WGBS)

Genomic DNA from iMEF A cells was bisulfite-converted using the EZ DNA Methylation-Gold kit (Zymo Research) according to the manufacturer's instructions. Libraries were prepared using Accel-NGS Methyl-Seq DNA Library Kit (Swift Biosciences) according to the manufacturer's instructions and sequenced on an Illumina Novaseq 6000 (PE100).

Libraries were aligned to mm10 using Bismark Mapper (0.22.1) with default parameters. PCR duplicates were subsequently removed with Bismark Deduplicate (0.22.1). Per-base methylation metrics were extracted using MethylDackel (0.3.0.1) with the following parameters: --OT 4,0,0,94 --OB 3,100,8,0 --keepSingleton --keepDiscordant -q 10 -p 5 -D 2000 --minOppositeDepth 0 --maxVariantFrac 1.0 -d 1 --ignoreFlags 3840 --requireFlags 0 –fraction.

Mathematical modeling

We simulate the PRC2 inhibition and washout/*Ezh2* deletion and rescue experiments, as well as the transient activation experiments, by exploring a mathematical model of a generic Polycomb target gene [52]. The simulations are conducted in the same way as in [52] using the direct Gillespie algorithm [93] where the methylation status of each H3 histone is simulated over time. In the simulations, there are four possible events: (1) the addition of a methyl group to a histone, (2) the removal of a methyl group from a histone, (3) replication and (4) transcription.

The addition of a methyl group to a histone H3 is described by the propensity function r_i^{me} (Table M2). When this process occurs in the simulation, an unmethylated histone transits to monomethylated, a monomethylated to dimethylated, etc.

The removal of methyl groups, demethylation, is described by r_i^{dem} and when demethylation is carried out a trimethylated histone is converted to dimethylated, a dimethylated to monomethylated etc.

When replication is carried out, the nucleosome is exchanged, with a probability of 0.5 per nucleosome, for a nucleosome with both histones unmethylated.

Table M2. Propensity functions. The propensity function for (1) adding methyl groups, r_i^{me}, (2) removing methyl groups, r_i^{dem}, (3) DNA replication and (4) transcription initiation f (see notations in Table M3).

	Propensity functions
1	$r_i^{me} = \beta(\delta_{s_i,me0}(\gamma_{me0-1} + k_{me0-1}E_i) + \delta_{s_i,me1}(\gamma_{me1-2} + k_{me1-2}E_i)$ $+ \delta_{s_i,me2}(\gamma_{me2-3} + k_{me}E_i))$
2	$r_i^{dem} = \gamma_{dem}(\delta_{s_i,me1} + \delta_{s_i,me2} + \delta_{s_i,me3})$
3	With probability $\frac{1}{2}$: $S_j S_{j+1} \to me0me0$ for $j = 1,3,5,\dots,N-1$
4	$f = \begin{cases} \alpha\left(f_{max} - \dfrac{P_{\frac{me2}{me3}}}{P_T}(f_{max} - f_{min})\right), & P_{\frac{me2}{me3}} < P_T \\ \alpha(f_{min}), & P_{\frac{me2}{me3}} \geq P_T \end{cases}$ If $f > f_{lim}$ then set $= f_{lim}$.

Transcription initiation is described by the step-wise linear function f. When transcription initiation is carried out in the simulations, the histones are exposed to demethylation and histone exchange. The histones are demethylated (as described above) with a probability of p_{dem} per histone and exchanged with a probability of p_{ex} per histone. When a histone is exchanged, both histones of a nucleosome are changed to unmethylated (histone i and $i + 1$ if i is odd, histone i and $i - 1$ if i is even).

The notation and equations are further explained in Table M3. The justifications, assumptions and detailed implementation for the propensity functions are described in more detail in [52].

Table M3. Explanations of notations. Descriptions and definitions of the notation used in the propensity functions.

Notation	Description
$i \in [1, N]$	H3 histones (N even)
$S_i \in [me0, me1, me2, me3]$	The methylation status of each histone i
$\delta_{x,y} = \begin{cases} 1, x = y \\ 0, x \neq y \end{cases}$	Kronecker delta
$E_i = \sum_{j \in M_i} (\rho_{me2}\delta_{s_j,me2} + \delta_{s_j,me3})$	The influence of neighboring histones
$M_i = \begin{cases} \{i-3, i-2, i-1, i+1, i+2\}, & i \text{ even} \\ \{i-2, i-1, i+1, i+2, i+3\}, & i \text{ odd} \end{cases}$	Neighboring histones
$P_{me2/me3} = \dfrac{1}{N}\sum_{j=1}^{N}(\delta_{s_j,me2} + \delta_{s_j,me3})$	Proportion of me2/me3 marks

Two important parameters: α and β
To modulate the transcription strength and the *trans*-factor-mediated regulation of gene expression we explore the parameter α. The parameter is encoded in the transcription initiation function f (Table M2), α = 1 is neutral, α < 1 is repressive and α > 1 is activating.

The parameter β describes the strength of the local PRC2 activity and is incorporated in the propensity r_i^{me} (Table M2). The higher the value of β, the higher the probability of adding methyl groups. When β << 1, the gene is not a PRC2 target and will have low simulated H3K27me3 levels.

Parameters and simulation outputs
The parameters we use from [52] are listed in Table M4. These are fixed during all simulations. The parameters α and β are free and vary between the different conditions that are simulated.

Table M4. The model parameters chosen from [52] that are fixed for all simulations.

Parameter	Description	Value
N	Number of histones	60
	Cell cycle length (h)	22
k_{me}	PRC2-mediated methylation rate (me2 to me3) (histone-1s-1)	$8 \cdot 10^{-6}$
k_{me0-1}	PRC2-mediated methylation rate (me0 to me1) (histone-1s-1)	$9k_{me}$
k_{me1-2}	PRC2-mediated methylation rate (me1 to me2) (histone-1s-1)	$6k_{me}$
γ_{me0-1}	Noisy methylation rate (me0 to me1) (histone-1s-1)	$k_{me0-1}/20$
γ_{me1-2}	Noisy methylation rate (me1 to me2) (histone-1s-1)	$k_{me1-2}/20$
γ_{me2-3}	Noisy methylation rate (me2 to me3) (histone-1s-1)	$k_{me}/20$
ρ_{me2}	Relative activation of PRC2 by H3K27me2	1/10
f_{min}	Minimum transcription initiation rate (s-1)	10^{-4}
f_{max}	Maximum transcription initiation rate (s-1)	$4 \cdot 10^{-3}$
ρ_{dem}	Demethylation probability (histone-1transcription-1)	$4 \cdot 10^{-3}$
ρ_{ex}	Histone exchange probability (histone-1transcription-1)	10^{-3}
γ_{dem}	Noisy demethylation rate (histone-1s-1)	$f_{min}\rho_{dem}$
P_T	Threshold proportion of me2/me3 for maximum repression	1/3
f_{lim}	Limit on maximum transcription initiation (s-1)	1/60

The simulation of a specific set of α and β, (α_0,β_0), is referred to as a "simulated gene." The output of the simulations used in the main text is time (in cell cycles), H3K27me3 and transcriptional output. When the different conditions listed in Table M6 are simulated for Fig. 3b, the transcriptional initiation events per hour are recorded and averaged over the N_{gen}th cell cycle. The H3K27me3 levels are the average levels (fraction of maximum) across the simulated gene immediately before replication in the N_{gen}th cell cycle. For the simulations of Fig. 3d, H3K27me3 levels and transcriptional initiation events per hour are recorded throughout the cell cycle. All the respective outputs are then averaged over the N_{sim} times they have been simulated (Table M5).

In the Gillespie algorithm, the time steps are not constant; we therefore convert the H3K27me3 levels in the Gillespie output to the H3K27me3 levels that would have been recorded within a simulation with a constant time step. We do so by choosing a time step t_{out} and assigning it to the H3K27me3 levels recorded at the end of that time step within the Gillespie simulation.

Table M5. Additional parameters for the simulated experiments.

Parameter	Description	Value
N_{sim}	Number of simulations for a gene	1000
N_{gen}	Number of cell cycles per condition	20
t_{out}	Time step for time course averaging (h)	1

Simulated experiments
For each of these conditions, the wild-type gene is first pre-simulated for N_{gen} cell cycles (starting from an initial condition of full methylation) and then each subsequent condition is simulated for N_{gen} cell cycles consecutively. The parameter β is changed between the different conditions in the simulated wild-type, PRC2 disruption and rescue experiment (Table M6).

Table M6. Simulated PRC2 disruption and rescue experiment. The corresponding value for α and β for each condition.

Parameter	Wild-type	PRC2 perturbation PRC2 inhibition/ *Ezh2*$^{-/-}$	PRC2 restoration Inhibitor washout/ *Ezh2* rescue
α	α_0	α_0	α_0
β	β_0	0	β_0

The parameter α is changed between the different conditions in the transient transcriptional activation and washout experiment (Table M7).

Table M7. The transient transcriptional activation and washout experiment. The corresponding value of α and β for each condition.

Parameter	Wild-type	Transcriptional perturbation Transient activation	Transcriptional restoration Activator washout
α	α_0	α_{max}	α_0
β	β_0	β_0	β_0

Classification of simulated genes
To classify the genes into reversible, irreversible and intermediate we use the following criteria:

I. Upregulation in perturbation v. wild-type ($\frac{Transcription_{perturbation}}{Transcription_{WT}} > 2$).

II. Upregulation in perturbation v. restoration ($\frac{Transcription_{perturbation}}{Transcription_{restoration}} > 2$).

III. Upregulation in restoration v. wild-type ($\frac{Transcription_{restoration}}{Transcription_{WT}} > 2$).

Irreversible genes fulfill criteria I and III (but not II); *reversible* fulfill I and II (but not III). The genes that don't fulfill the criteria for either irreversible or reversible are classified as *intermediate*.

Varying α and β
When α and β are varied in Fig. 3b, the values are logarithmically distributed over values of α and β that correspond to reversible or irreversible genes according to the classification above. The simulations in Extended Data Fig. 7d result from a similar protocol as for Fig. 3b, except that α and β are kept at constant values (α = 3.5, β = 2.1) and the duration of each cell cycle was varied within a PRC2 disruption phase of fixed total duration (440 h). The simulated transcriptional output in Fig. 3c results from the simulation output in the PRC2 disruption condition of Fig. 3b. The simulated H3K27me3 levels in Extended Data Fig. 7e result from the simulation output in the wild-type condition of Fig. 3b. We verified that these results were substantially unchanged when parameter values were sampled linearly rather than logarithmically. The simulations in Extended Data Fig. 10d result from a similar protocol as for Fig. 3d, except that the number of cell cycles of transient activation was varied.

Individual gene activation assays in iMEFs
A stable DD-dCas9-VPR-expressing iMEF B line (iMEF B-VPR) was obtained by co-transfecting iMEF B cells with pCMV-hyPBase and varying amounts of PB-TRE-FKBP12DD-dCas9-VPR, selecting with 0.4 mg/mL hygromycin B and isolating clones from the conditions with the least PB-TRE-FKBP12DD-dCas9-VPR that produced hygromycin-resistant transfectants. Clones were tested for inducible DD-dCas9-VPR

expression by treatment with 1 μg/mL doxycycline followed by reverse transcription and quantitative PCR analysis, and chosen for use in the study on the basis of high fold-induction and low basal expression.

Ezh2 KO iMEF B-VPR cells were obtained by treatment with 100 nM 4-hydroxytamoxifen (Sigma). iMEF B-VPR lines with genetic deletions other than *Ezh2* were obtained by co-transfection of appropriate pLKO.1-blast-dual-guide constructs and hCas9-without-neo (most deletions), or transfection of the appropriate pX458 (*Crebbp* and *Foxa1*), followed by clone isolation by limiting dilution without antibiotic selection and screening by PCR for homozygous gene disruption. Sequences of gRNAs used are listed in Extended Data Table 4.

Stable pools of DD-dCas9-VPR iMEFs for inducible activation of individual genes were obtained by transducing iMEF B-VPR cells, or genetic deletion clones thence derived, with lentiviruses assembled using pLKO.1-blast-dual-guide constructs containing gRNA sequences targeting the region immediately upstream of the transcription start site (listed in Extended Data Table 4), and by selecting transductants in bulk with 3.5 μg/mL blasticidin.

Gene activation was achieved by treating cells with 1 μg/mL doxycycline and 1 mM Shield-1 (AOBIOUS).

Deletion of DD-dCas9-VPR after activation assays in iMEF B-VPR cells was achieved by co-transfection of hCas9-PID-NAA-BPNLS and a pLKO.1-blast-dual-guide construct containing gRNA sequences targeting sites flanking the DD-dCas9-VPR with NAA as the protospacer-adjacent motif (PAM). Genomically integrated sgRNAs for genes induced in the activation assay, which target sites bearing the conventional NGG PAM, are not expected to enable cleavage by the transfected Cas9 with the modified PAM-interacting domain (PID). Clones were isolated by limiting dilution without antibiotic selection and screened for excision or early frameshift of DD-dCas9-VPR, which were confirmed by anti-Cas9 Western blot after treatment with 1 μg/mL doxycycline and 1 mM Shield-1.

<u>Reverse transcription for quantitative PCR and sequencing of RT-PCR products</u>
RNA from was extracted from cell pellets using the RNeasy mini kit (Qiagen) according to the manufacturer's instructions and reverse transcribed using the High-Capacity cDNA Reverse Transcription kit (Applied Biosystems) according to the manufacturer's instructions.

Quantitative PCR
qPCR was carried out on an Applied Biosystems ViiA 7 instrument (primers listed in Extended Data Table 3; normalization was performed using *Tbp*).

<u>5-aza-2'-deoxycytidine treatment and LUMA assay</u>
5-aza-2'-deoxycytidine was purchased from Sigma and re-supplied daily to cells undergoing treatment. LUminometric Methylation Assay to confirm reduction in global CpG methylation was conducted as previously described [94].

<u>Generation and isolation of heterokaryon clones</u>
Prior to cell fusion, iMEF B cells expressing mutant (OFF-state) alleles of *Nr2f1* or *Foxa1* were transduced with a lentiviral vector (produced from pCDH-CMV-EF1α-Flag-neo) conferring resistance to G418. iMEF B cells expressing wild-type (ON-state) of *Nr2f1* or *Foxa1* expressed the blasticidin resistance gene present on the sgRNA expression vector. 390 000 iMEF B cells of each transcriptional ON or OFF state were plated together in the same well of a 6-well plate and allowed to attach for a few hours. Cells were washed twice with warm (37°C) PBS and incubated 1 min in 50% PEG-1500 (w/v) in 75 mM Hepes (pH 8.0) (Sigma). 3 mL of PBS was added gradually to dilute PEG, followed by 2 washes with PBS and 1 wash with culture medium. The following day, cells were

trypsinized and plated in limiting dilutions in 10-cm plates in the presence of 4 ug/mL blasticidin and 1.3 mg/mL G418 to select individual heterokaryon clones.

DAPI/rhodamine-phalloidin staining
Cells were fixed in 4% paraformaldehyde for 5 minutes at room temperature. Following a wash in PBS, cells were permeabilized in PBS containing 0.5 % Triton X-100 for 5 min at room temperature and then blocked in PBS containing 20 % goat serum for 30 min at room temperature. Cells were then washed once in incubation buffer (PBS containing 0.001% Tween-20, 0.1% BSA and 1 mM sodium azide) followed by a 90-minute incubation with incubation buffer containing DAPI and rhodamine-phalloidin. Cells were then washed 3 times in PBS and mounted with Vectashield (Vectorlabs) for fluorescent imaging.

Next-generation sequencing of reverse-transcription-PCR products
Sequences were amplified from cDNA using the primers GAGCGTCCGCAGGAACTTAACT and CTGCATGCACTGGCTGCCATAA (*Nr2f1*) or those listed for quantitative PCR in Extended Data Table 3 (*Foxa1*), and libraries were constructed using primers beginning with Illumina adapters and indexes and ending with CAATCCAGGCCAGTATGCACTC and CTGCATGCACTGGCTGCCATAA (*Nr2f1*) or with the sequences of the quantitative PCR primers (*Foxa1*). Sequencing was carried out by the Institut Curie Next Generation Sequencing Core Facility on an Illumina Miseq using Reagent Nano Kit v2 (PE150).
        Reads were classified according to whether they contained a perfect match for *Nr2f1* wild-type (CAATCCAGGCCAGTATGCACTCA<u>CAAA</u>CGGGGATCCTCTCAATGGCCACTGCTACCTGTC), *Nr2f1* mutant (CAATCCAGGCCAGTATGCACTCA<u>CAA</u>CGGGGATCCTCTCAATGGCCACTGCTACCTGTC or CAATCCAGGCCAGTATGCACTCA<u>CAATGGCTACATTTCTCTGCTGCTGCGCGCAGAGCCC</u>), *Foxa1* wild-type (ATGTTGCCGCTCGTGGTCATGGTGTTCAT<u>GGTCATGTAGG</u>TGTTCATGGAGTTCATAGAG) or *Foxa1* mutant (ATGTTGCCGCTCGTGGTCATGGTGTTCAT<u>GGG</u>TGTTCATGGAGTTCATAGAG or ATGTTGCCGCTCGTGGTCATGGTGTTCAT<u>GGTCAATGTAGG</u>TGTTCATGGAGTTCATAGAG) sequences.

Statistics and reproducibility
All measurements and statistical analyses involve distinct samples from independent experiments. All statistical tests are two-sided.

Data availability

The mass spectrometry PRM data that support the findings of this study have been deposited in the ProteomeXchange Consortium via the PRIDE [95] partner repository with the dataset identifier PXD023966. They are accessible prior to publication (username = <u>reviewer_pxd023966@ebi.ac.uk</u>, password = hBp0DTzW). The CUT&RUN-seq, ChIP-seq, RNA-seq, ATAC-seq and WGBS data that support the findings of this study have been deposited in the Gene Expression Omnibus under the accession code GSE147568.

Code availability

All custom computer code developed for this study will be made available upon request.

References

69.   Scheuermann, J. C. *et al.* Histone H2A deubiquitinase activity of the Poly-comb repressive complex PR-DUB. *Nature* **465,** 243–247 (2010).

70.   Mali, P. *et al.* RNA-guided human genome engineering via Cas9. *Science* **339,** 823–826 (2013).

71.   Wassef, M. *et al.* Versatile and precise gene-targeting strategies for func-tional studies in mammalian cell lines. *Methods* **121-122,** 45–54 (2017).

72.   Yusa, K., Zhou, L., Li, M. A., Bradley, A. & Craig, N. L. A hyperactive piggyBac transposase for mammalian applications. *Proceedings of the National Acad-emy of Sciences* **108,** 1531–1536 (2011).

73.   Kearns, N. A. *et al.* Cas9 effector-mediated regulation of transcription and differentiation in human pluripotent stem cells. *Development* **141,** 219–223 (2014).

74.   Vidigal, J. A. & Ventura, A. Rapid and efficient one-step generation of paired gRNA CRISPR-Cas9 libraries. *Nature Communications* **6,** 8083–7 (2015).

75.   Ran, F. A. *et al.* Genome engineering using the CRISPR-Cas9 system. *Nat Protoc* **8,** 2281–2308 (2013).

76.   Chatterjee, P. *et al.* A Cas9 with PAM recognition for adenine dinucleotides. *Nature Communications* **11,** 2474 (2020).

77.   Koblan, L. W. *et al.* Improving cytidine and adenine base editors by expres-sion optimization and ancestral reconstruction. *Nat Biotechnol* **36,** 843–846 (2018).

78.   Suzuki, K. *et al.* In vivo genome editing via CRISPR/Cas9 mediated homolo-gy-independent targeted integration. *Nature* **540,** 144–149 (2016).

79.   Conti, L. *et al.* Niche-independent symmetrical self-renewal of a mammalian tissue stem cell. *Plos Biol* **3,** e283 (2005).

80.   Gendrel, A.-V. *et al.* Developmental dynamics and disease potential of ran-dom monoallelic gene expression. *Dev Cell* **28,** 366–380 (2014).

81.   Wassef, M., Michaud, A. & Margueron, R. Association between EZH2 expres-sion, silencing of tumor suppressors and disease outcome in solid tumors. *Cell Cycle* **15,** 2256–2262 (2016).

82.   Molden, R. C. & Garcia, B. A. Middle-Down and Top-Down Mass Spectromet-ric Analysis of Co-occurring Histone Modifications. *Curr Protoc Protein Sci* **77,** 23.7.1–28 (2014).

83.   Poullet, P., Carpentier, S. & Barillot, E. myProMS, a web server for manage-ment and validation of mass spectrometry-based proteomic data. *Prote-omics* **7,** 2553–2556 (2007).

84.   Skene, P. J., Henikoff, J. G. & Henikoff, S. Targeted in situ genome-wide pro-filing with high efficiency for low cell numbers. *Nat Protoc* **13,** 1006–1019 (2018).

85.   Saldanha, A. J. Java Treeview--extensible visualization of microarray data. *Bioinformatics* **20,** 3246–3248 (2004).

86.   Buenrostro, J. D., Wu, B., Chang, H. Y. & Greenleaf, W. J. ATAC-seq: A Method for Assaying Chromatin Accessibility Genome-Wide. *Curr Protoc Mol Biol* **109,** 21.29.1–21.29.9 (2015).

87.   Karabacak Calviello, A., Hirsekorn, A., Wurmus, R., Yusuf, D. & Ohler, U. Re-producible inference of transcription factor footprints in ATAC-seq and DNase-seq datasets using protocol-specific bias modeling. *Genome Biol* **20,** 42–13 (2019).

88.   Meers, M. P., Tenenbaum, D. & Henikoff, S. Peak calling by Sparse Enrich-ment Analysis for CUT&RUN chromatin profiling. *Epigenetics Chromatin* **12,** 42–11 (2019).

89.   Eden, E., Navon, R., Steinfeld, I., Lipson, D. & Yakhini, Z. GOrilla: a tool for

discovery and visualization of enriched GO terms in ranked gene lists. *BMC Bioinformatics* **10,** 48 (2009).

90.   Supek, F., Bošnjak, M., Škunca, N. & Šmuc, T. REVIGO summarizes and visualizes long lists of gene ontology terms. *PLoS ONE* **6,** e21800 (2011).

91.   Heinz, S. *et al.* Simple combinations of lineage-determining transcription factors prime cis-regulatory elements required for macrophage and B cell identities. *Molecular Cell* **38,** 576–589 (2010).

92.   Castro-Mondragon, J. A., Jaeger, S., Thieffry, D., Thomas-Chollier, M. & van Helden, J. RSAT matrix-clustering: dynamic exploration and redundancy reduction of transcription factor binding motif collections. *Nucleic Acids Res* **45,** e119 (2017).

93.   Gillespie, D. T. Exact stochastic simulation of coupled chemical reactions. *J. Phys. Chem.* **81,** 2340–2361 (1977).

94.   Karimi, M. *et al.* LUMA (LUminometric Methylation Assay)--a high throughput method to the analysis of genomic DNA methylation. *Experimental Cell Research* **312,** 1989–1995 (2006).

95.   Perez-Riverol, Y. *et al.* The PRIDE database and related tools and resources in 2019: improving support for quantification data. *Nucleic Acids Res* **47,** D442–D450 (2019).
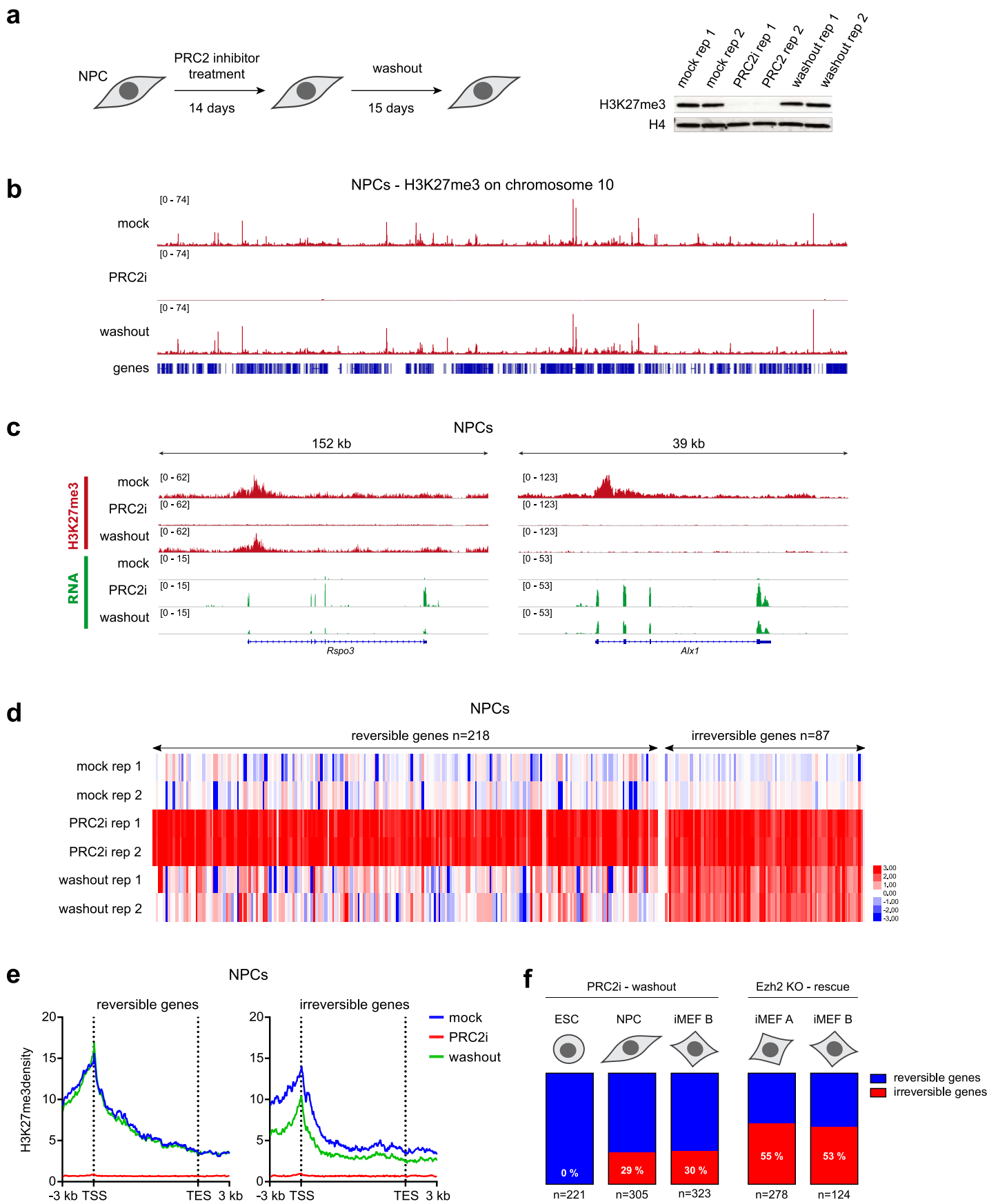
Fig. 1. Transient disruption of PRC2 triggers permanent activation of a large subset of repressed target genes. a, Schematic of transient PRC2 inhibition experiment and Western blot analysis of nuclear extracts from the indicated conditions. NPC, mouse neural progenitor cells. PRC2i, PRC2 inhibition with 2 μM UNC1999 and 4 μM A-395. **b**, Tracks of H3K27me3 CUT&RUN for the indicated conditions over entire chromosome 10 in NPCs. **c**, Tracks of H3K27me3 CUT&RUN and RNA-seq for the indicated conditions at representative genes reversibly (*Rspo3*) or irreversibly (*Alx1*) activated upon transient disruption of PRC2 in NPCs. **d**, Heatmap of RNA-seq levels (log2 fold change with respect to the mean of the two mock replicates) in the indicated conditions for the full sets of reversible and irreversible PRC2 target genes. **e**, Metaplots of average H3K27me3 CUT&RUN density over the interval from TSS − 3 kb to TES + 3 kb for the full sets of reversible and irreversible PRC2 target genes in the indicated conditions. TSS, transcription start site. TES, transcription end site. **f**, Relative proportions of reversible and irreversible genes in ESCs, NPCs and iMEF line B after treatment with PRC2 inhibitors and washout, and in iMEF lines A and B after genetic deletion of *Ezh2* followed by *Ezh2* rescue. The total number of genes (reversible + irreversible) is indicated at the bottom and the percentage of irreversible genes is indicated in white on each graph. ESC, mouse embryonic stem cells. iMEF, immortalized mouse embryonic fibroblasts.
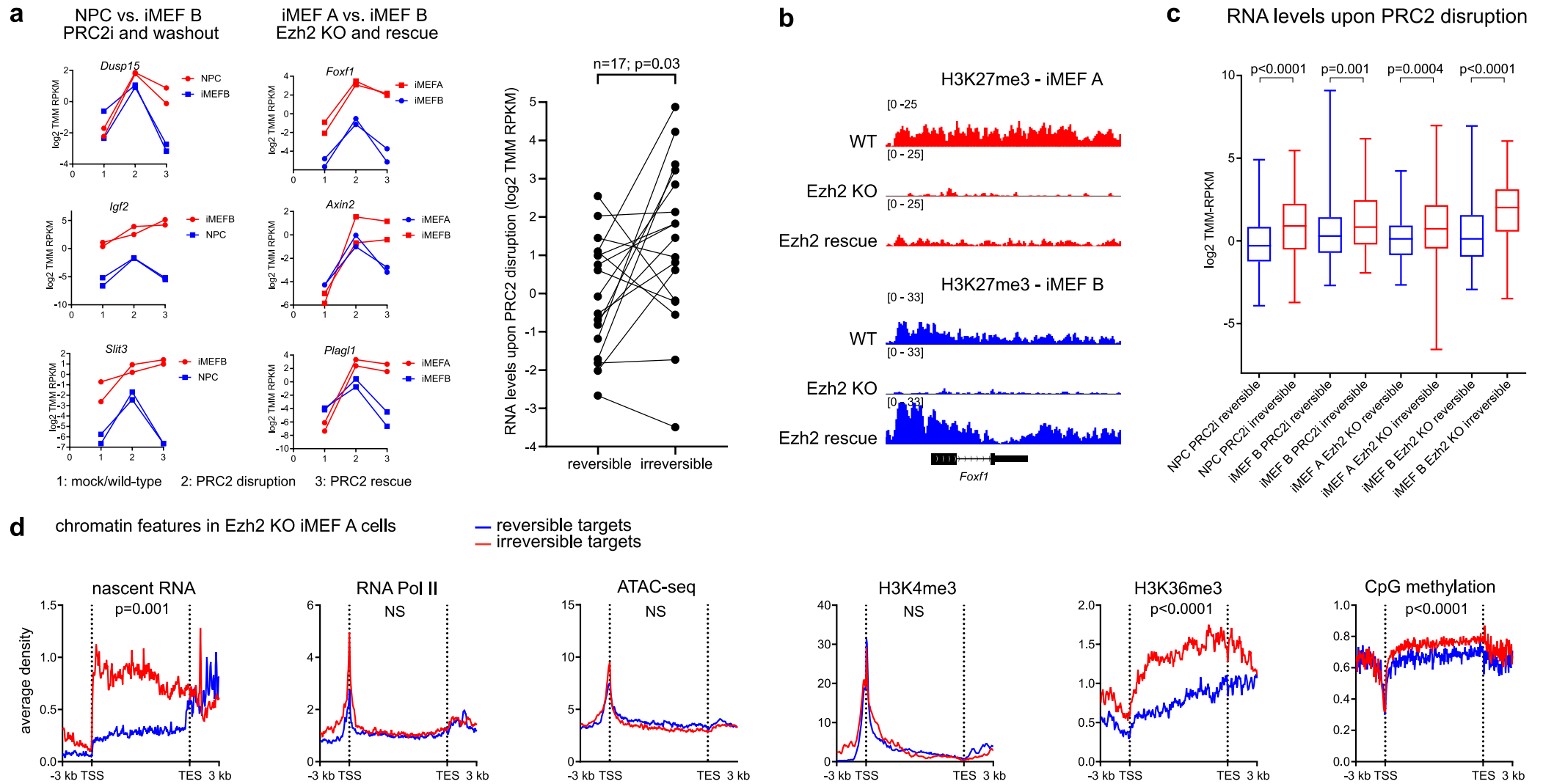
Fig. 2. Stable epigenetic switching of target genes is correlated to level of transcriptional activity upon disruption of PRC2. a, Left, RNA levels of individual genes classified differentially as reversible and irreversible in different cell lines subjected to the same treatment as indicated. The cell line in which the gene is reversible is represented in blue and that in which it is irreversible is represented in red. TMM-RPKM, trimmed mean of M-values-reads per kilobase per million. PRC2i, PRC2 inhibition with 2 μM UNC1999 and 4 μM A-395. Right, RNA levels in PRC2 disruption condition of every gene classified differentially as reversible and irreversible in different cell lines subjected to the same treatment. For each gene, a line connects the value for the cell line in which the gene is reversible to that for the cell line in which it is irreversible. The p-value is the result of a Wilcoxon matched-pairs signed rank test. **b**, Tracks of H3K27me3 ChIP-seq in iMEF A and iMEF B cells for the indicated conditions at the *Foxf1* locus. **c**, Box plots (median, lower and upper quartiles, lowest and highest values) of RNA levels of all reversible and irreversible genes in the indicated cell lines upon disruption of PRC2 activity. p-values are the results of Mann–Whitney tests comparing irreversible and reversible genes for each cell line. Difference between medians (Hodges-Lehmann) are: 1.05 (CI 0.62-1.52) for NPC, 0.66 (CI 0.26-1.07) for iMEF B PRC2i, 0.77 (CI 0.36-1.19) for iMEF A Ezh2 KO and 1.56 (CI 0.81-2.22) for iMEF B Ezh2 KO. CI, confidence interval. **d**, Metaplots of average nascent RNA, RNA Pol II ChIP-seq, ATAC-seq, H3K4me3 ChIP-seq, H3K36me3 ChIP-seq and CpG methylation density over the interval from TSS – 3 kb to TES + 3 kb for the full sets of reversible and irreversible PRC2 target genes in iMEF A *Ezh2* deletion cells. p-values are the results of Mann–Whitney tests comparing irreversible and reversible genes for each feature. NS, not significant.
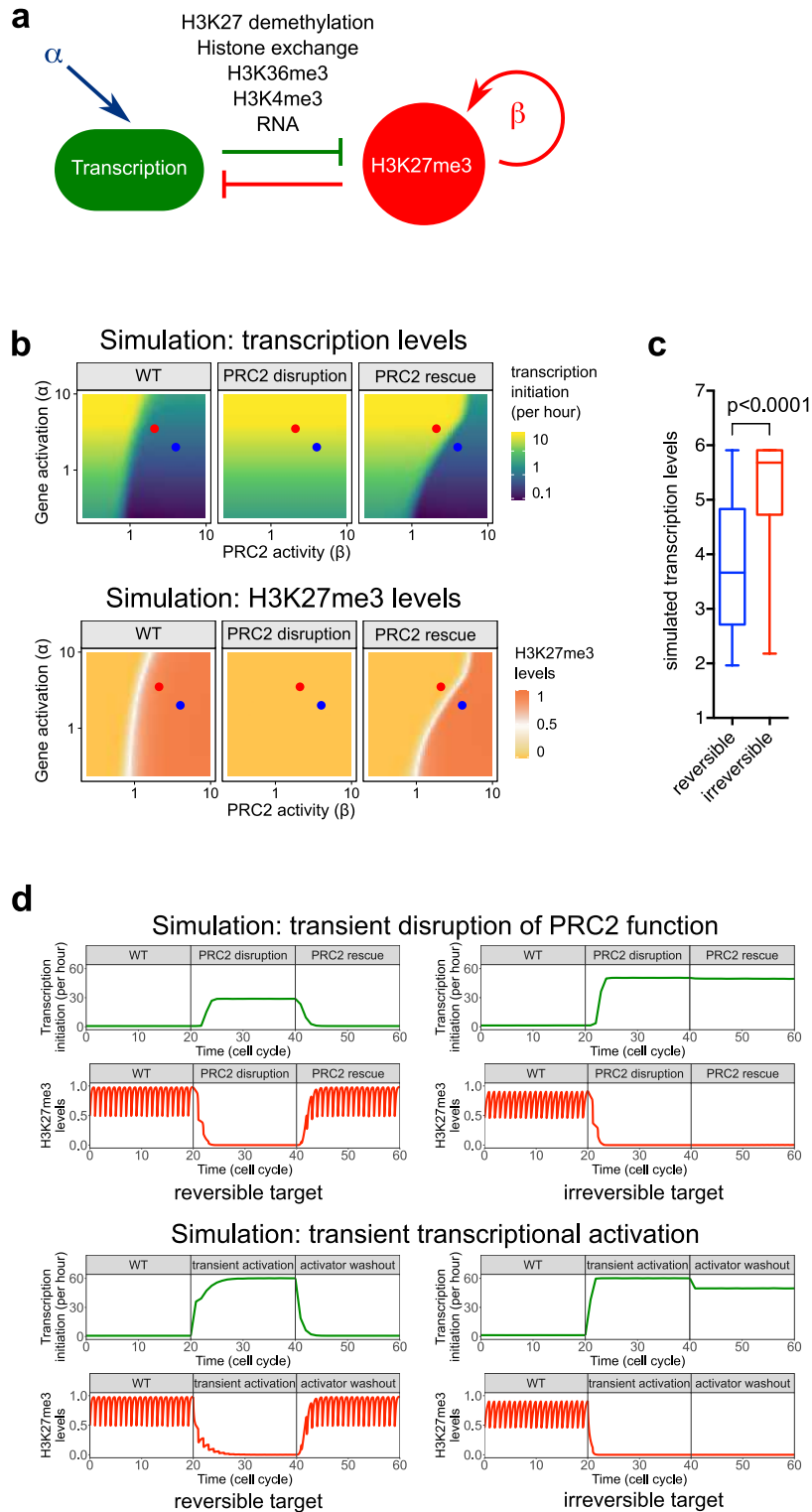
Fig. 3. Computational simulations predict conditions required for stable epigenetic switching in response to transient stimuli. a, Schematic of theoretical model formalizing a mutual antagonism between transcriptional activity and PRC2 recruitment and activity[52]. α, intrinsic strength of *trans*-acting inputs promoting transcriptional activity of a given gene. β, intrinsic strength of targeting and modification of a given gene locus by PRC2. **b**, Heatmaps depicting mean transcription initiation events per hour and H3K27me3 levels obtained upon simulating the indicated conditions consecutively for 20 cell cycles each across a range of values of α and β (see Methods). Blue circle, (wild-type: $\alpha=\alpha_0=2$, $\beta=\beta_0=4$) pair predicted to result in reversible activation upon transient disruption of PRC2; red circle, (wild-type: $\alpha=\alpha_0=3.5$, $\beta=\beta_0=2.1$) pair predicted to result in irreversible activation upon transient disruption of PRC2. **c**, Box plots comparing irreversible and reversible genes for simulated transcription initiation events per hour. p-value for Mann-Whitney test is displayed. Difference between medians (Hodges-Lehmann): 1.5 (CI 1.4-1.7). The levels are from the PRC2 disruption simulations in **b** (middle), with parameter values sampled logarithmically over parameter space (see Methods). CI, confidence interval. **d**, Top, graphs depicting the transcription (transcription initiation events per hour) and H3K27me3 levels tracked over 20 simulated cell cycles of each of the indicated conditions, for the two (α_0, β_0) pairs from **b** corresponding to reversible and irreversible gene activation, respectively. Bottom, graphs depicting the levels of transcription and H3K27me3 tracked over 20 simulated cell cycles each before, during and after a transient pulse of transcriptional activation with $\alpha=\alpha_{max}=100$ for otherwise the same two (α_0, β_0) pairs. Note the wave pattern for H3K27me3, which results from replicative dilution and gradual reacquisition at each cell cycle.
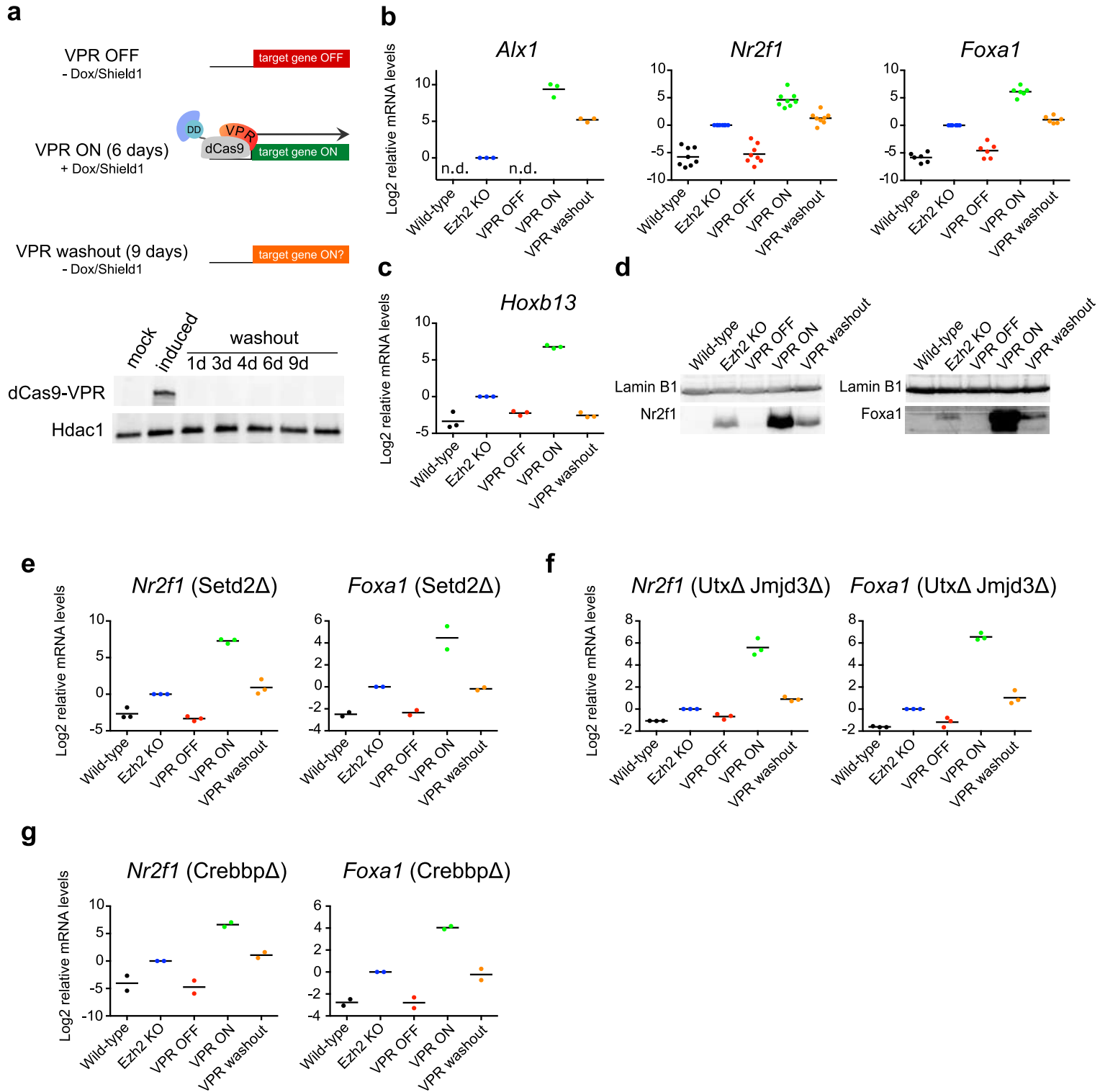
Fig. 4. Transient activation of individual PRC2 target genes can trigger permanent switching of transcriptional states. a, Schematic of transient activation assay in iMEF B cells and Western blot analysis of nuclear extracts from the indicated conditions. DD, FKBP12 destabilization domain[58,59], VPR, VP64-p65-Rta [57]. **b,c**, Messenger RNA levels of indicated target genes in cells bearing the DD-dCas9-VPR construct and either lacking (wild-type, Ezh2 KO) or constitutively expressing (VPR OFF, ON, washout) sgRNAs specific to the target gene. Values within each experiment are normalized to the Ezh2 KO condition. Horizontal lines represent mean values. n.d., not detected. **d**, Western blot analysis of nuclear extracts from the indicated conditions. **e**, As in **b** and **c**, but analyzing target genes in cells carrying a deletion in *Setd2*. **f**, As in **b** and **c**, but analyzing target genes in cells carrying deletions in *Utx* and *Jmjd3*. **g**, As in **b** and **c**, but analyzing target genes in cells carrying a deletion in *Crebbp*.
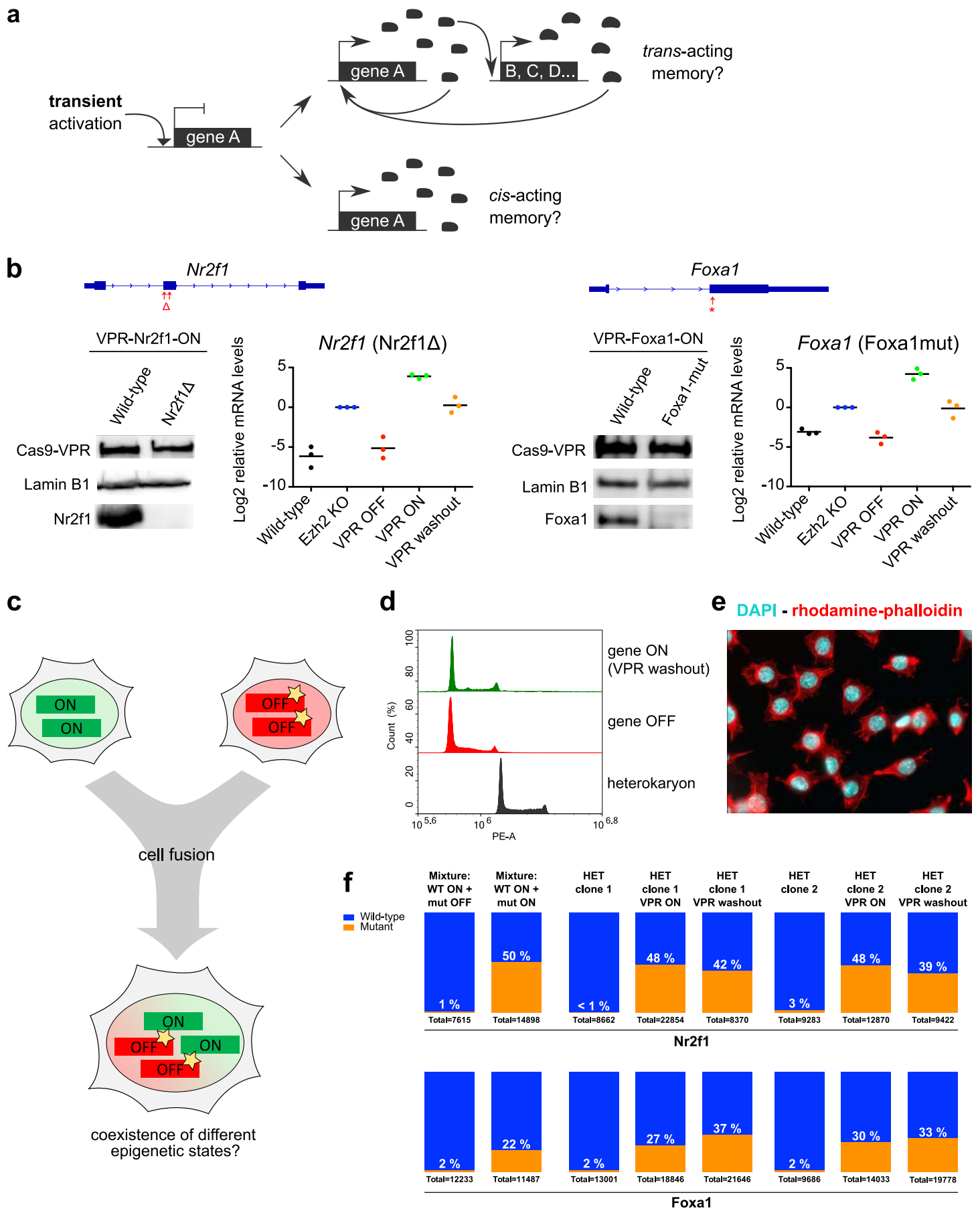
Fig. 5. A *cis*-acting mechanism creates a heritable record of activation at PRC2 target genes. **a**, Schematic illustrating alternative models of transcriptional memory in which activation of feedbacks involving transcription factors is required (*trans*) or in which activation of such feedbacks is dispensable (*cis*). **b**, Top, schematic of short deletion in *Nr2f1* and site of short indels in *Foxa1* predicted to result in frameshift mutations. Bottom (images), Western blot analysis of nuclear extracts from wild-type, *Nr2f1*-mutant and *Foxa1*-mutant cells cultured in dCas9-VPR-inducing conditions and expressing sgRNAs targeting *Nr2f1* or *Foxa1*, as indicated. Bottom (graphs), *Nr2f1* and *Foxa1* messenger RNA levels in cells mutant for the corresponding gene, carrying the DD-dCas9-VPR construct and either lacking (wild-type, Ezh2 KO) or constitutively expressing (VPR OFF, ON, washout) sgRNAs specific to the target gene and subjected to the experimental treatment depicted in Fig. 4a. Values within each experiment are normalized to the Ezh2 KO condition. Horizontal lines represent mean values. **c**, Schematic of cell fusion experiments between cells carrying PRC2 target genes in different transcriptional states. Cells in the ON state are obtained by transient activation of the target gene using dCas9-VPR. Cells in the OFF state carry the mutations shown in **b** in order to distinguish alleles within fused cells based on their initial expression state. **d**, Representative FACS analysis of propidium iodide-stained cells showing a doubling in ploidy between initial conditions and a heterokaryon clone. **e**, Micrograph of cells from a representative heterokaryon clone stained with DAPI (nucleus) and rhodamine-phalloidin (cytoskeleton). Note the presence of only one nucleus per cell. **f**, Read counts in next-generation sequencing of cDNA molecules spanning the mutation sites shown in **b**. Mixtures of equal quantities of total RNA from the indicated conditions, or total RNA from heterokaryons or heterokaryons subjected to indicated dCas9-VPR-mediated activation treatments, were used for RT-PCR reactions. The percentage of mutant reads is shown in white on each graph, and the total below each graph denotes the number of informative reads for the corresponding cDNA sample. HET, heterokaryon.
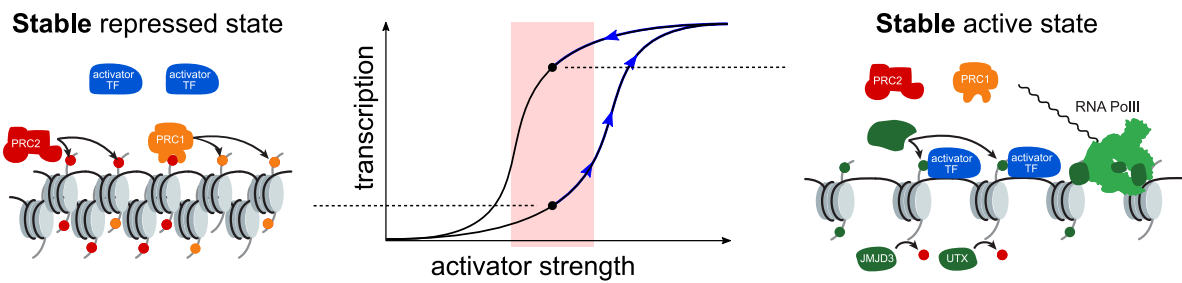
Fig. 6. Model of *cis*-acting transcriptional memory at PRC2 target genes. Mutual antagonism between PRC2 activity and the process of transcription enables transient events to produce mitotically heritable switches in expression states. Trajectory indicates dynamical response to a transient increase in activator strength, which irreversibly switches the gene from a low to a high transcriptional state. Red zone indicates region of activator strengths where bistable expression states are possible. PRC2-mediated transcriptional memory can operate in a gene-autonomous fashion and independently of *trans*-acting feedbacks.
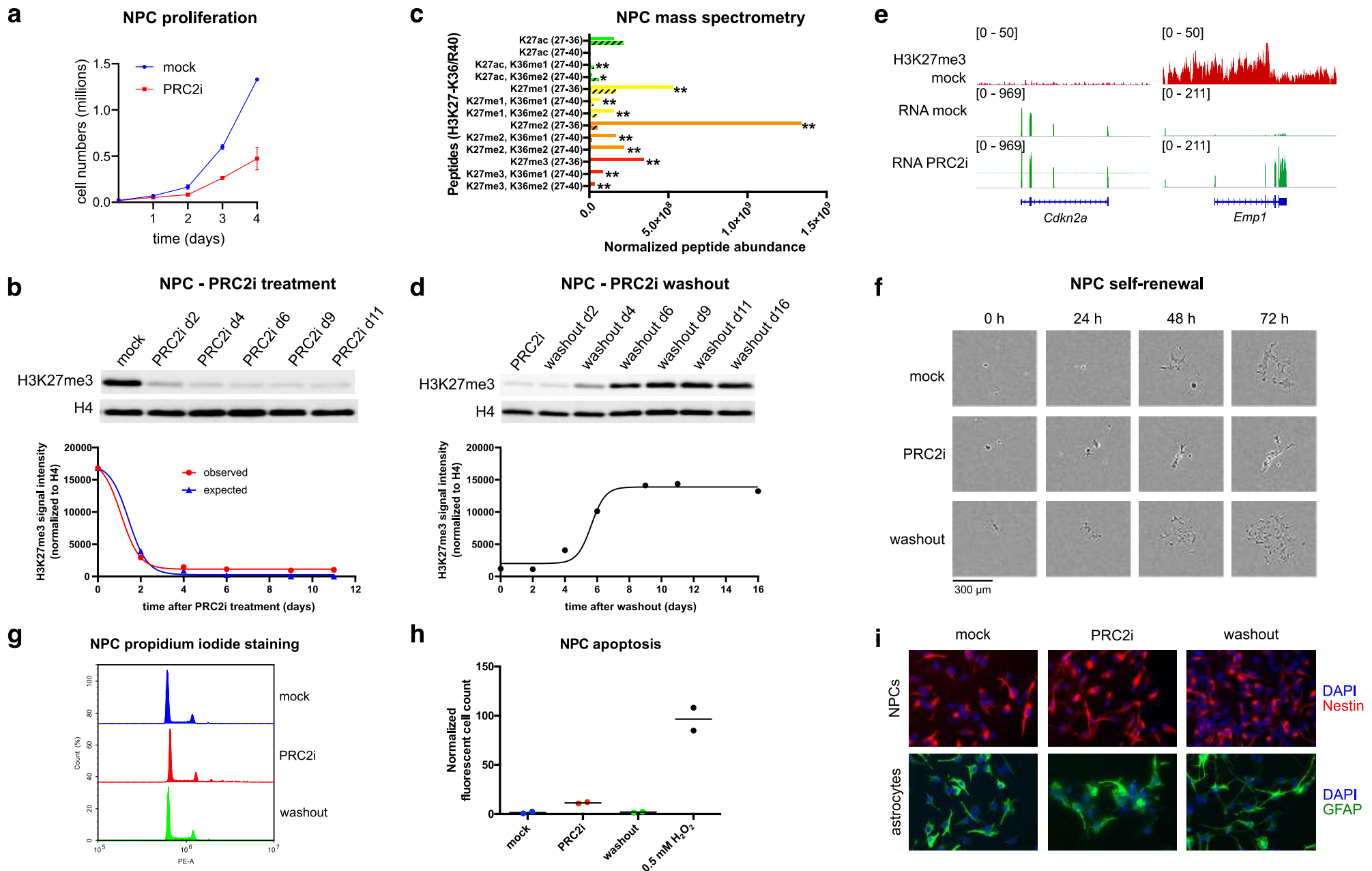
Extended Data Fig. 1. Neural progenitor cells treated with PRC2 inhibitors show potent loss of H3K27me3 and retain key physiological characteristics. a, Equal numbers of cells were seeded in multi-well plates on day 0 in the presence or absence of 2 μM UNC1999 and 4 μM A395 (hereafter PRC2i), and cells were counted at successive 24-hour intervals. Mean values of two experiments are shown; error bars indicate actual values obtained in each experiment. **b**, Top, Western blot of nuclear extracts from cells cultured in the presence of PRC2i for the indicated number of days using the indicated antibodies. Bottom, quantification of H3K27me3 Western blot signal, normalized to H4, in arbitrary units, plotted with an exponential regression model and compared to the levels expected assuming two-fold dilution per population doubling time as estimated from the data in **a**. **c**, Quantification of the indicated post-translationally modified peptides combined across histone H3.1, H3.2 and H3.3 by targeted mass spectrometry, normalized to the unmodified peptide STELLIR (residues 57-63), in arbitrary units, in mock-treated (plain bars) and PRC2i-treated (hatched bars) cells (* denotes a p-value < 0.05; ** denotes a p-value < 0.01). See also Extended Data Table 1. **d**, Top, as in **b** (top), but for cells cultured continuously in the presence of PRC2i or after a washout of the indicated number of days. Bottom, quantification of H3K27me3 Western blot signal, normalized to H4, in arbitrary units, plotted with a sigmoidal regression model. **e**, Tracks of H3K27me3 CUT&RUN and RNA-seq for the indicated conditions at the *Cdkn2a* locus (encoding p16INK4a and p19ARF proteins) in NPCs, showing lack of H3K27me3 signal (the *Emp1* gene is shown as a positive control). **f**, Cells in the indicated conditions were cultured in Incucyte device and imaged at the indicated times. **g**, Representative FACS analysis of propidium iodide-stained NPCs in the indicated conditions. **h**, Apoptosis assay carried out using Incucyte device to image cells in the indicated conditions in the presence of Caspase-3/7 Dye 12 h after plating. Fluorescent cell counts are normalized to cell confluence. **i**, Immunofluorescent staining of nestin and DAPI staining in neural progenitor cells subjected to the indicated treatments, and immunofluorescent staining of GFAP and DAPI staining in astrocytes differentiated from neural progenitor cells while undergoing the indicated treatments.
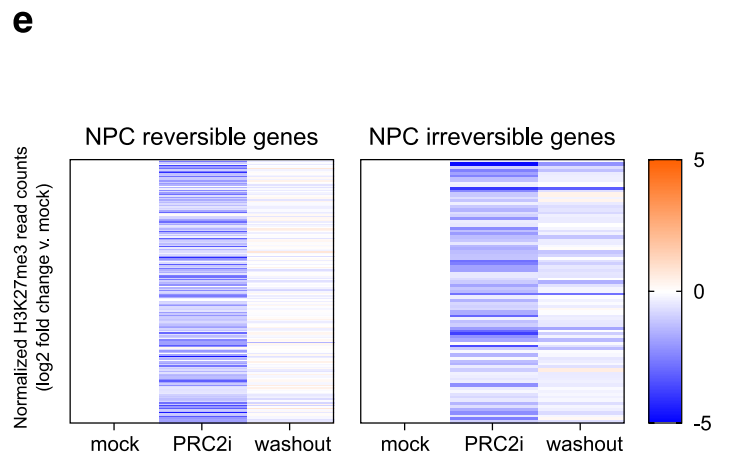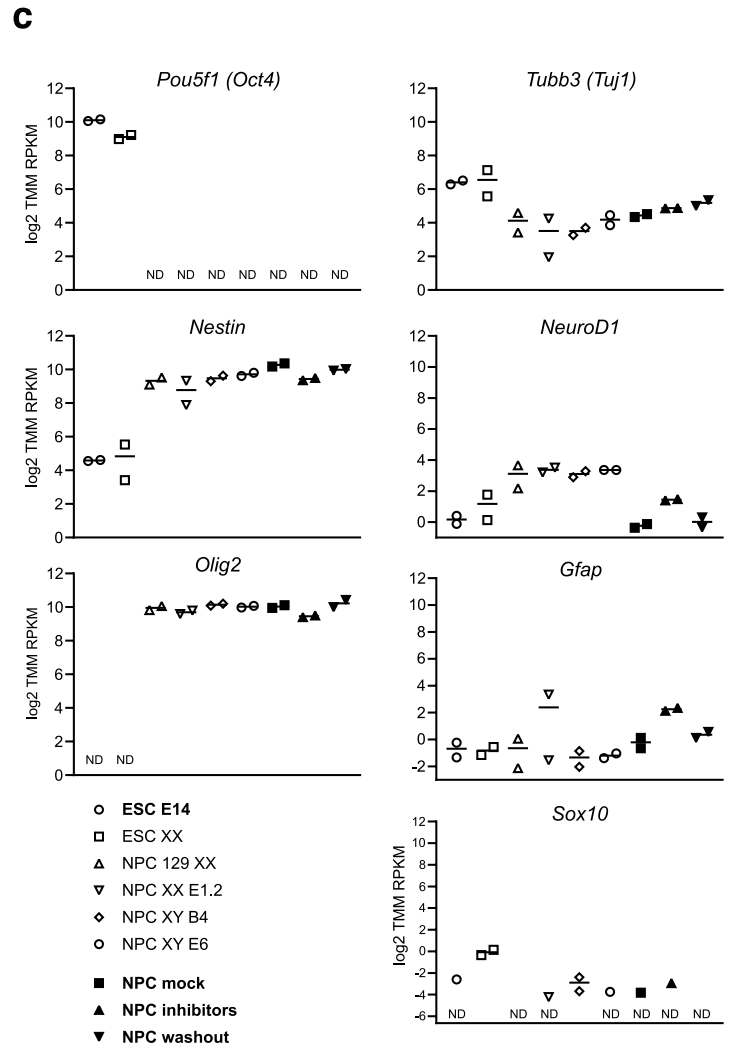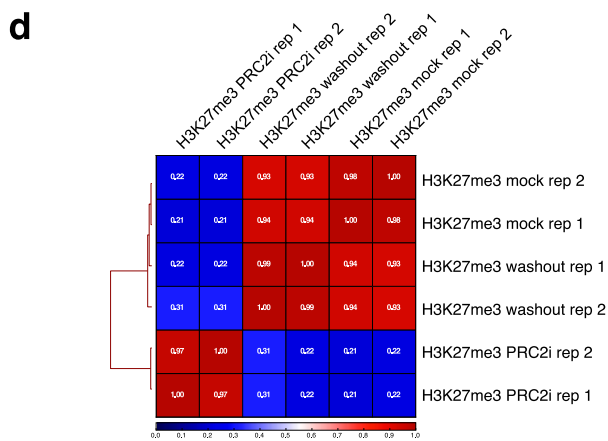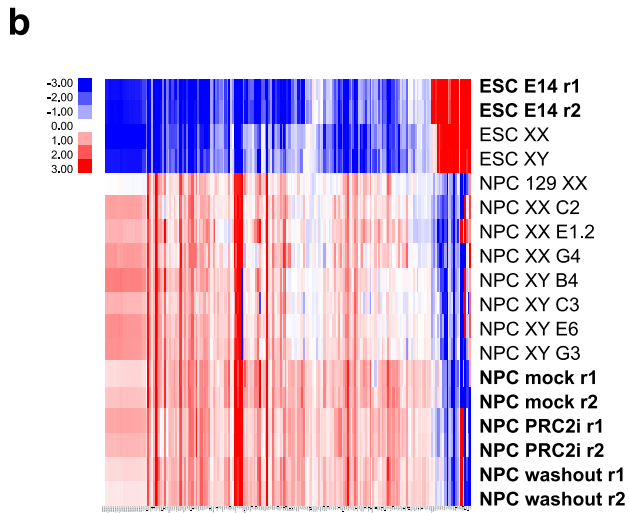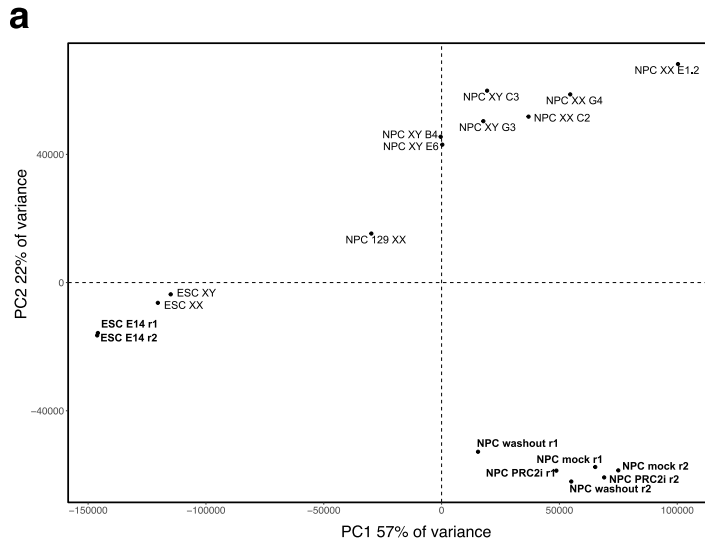
Extended Data Fig. 2. Neural progenitor cells treated with PRC2 inhibitors retain cell identiy markers and show robust rescue of H3K27me3 upon inhibitor washout. a-c, All samples analyzed are hybrid 129/Sv-Cast/EiJ, except where otherwise indicated: ESC E14 (129/Sv) and NPC 129 (129/Sv). Samples in bold are from this study; other samples are from [80]. **a**, Principal component analysis of the variance in RNA-seq counts mapping to exons among the indicated conditions. PRC2i, PRC2 inhibition with 2 μM UNC1999 and 4 μM A-395. **b**, Heatmap of RNA-seq levels in the indicated conditions for the set of 200 genes whose differential contribution to PC1 versus PC2 (the latter capturing experimental batch effects) in **a** was greatest (see Methods). Values for each gene represent the log2 fold differences with respect to the mean TMM-RPKM value of all samples. TMM-RPKM, trimmed mean of M-values-reads per kilobase per million. **c**, RNA-seq levels for the indicated lineage markers in the indicated conditions. ND, not detected. **d**, Matrix showing pairwise Pearson correlations of genomic read distributions for H3K27me3 CUT&RUN among the indicated conditions, listed in the order generated by unsupervised hierarchical clustering. **e**, Heatmap of normalized H3K27me3 CUT&RUN read counts (log2 fold change with respect to the mean of the two mock replicates) in the indicated conditions for the full sets of reversible and irreversible PRC2 target genes.
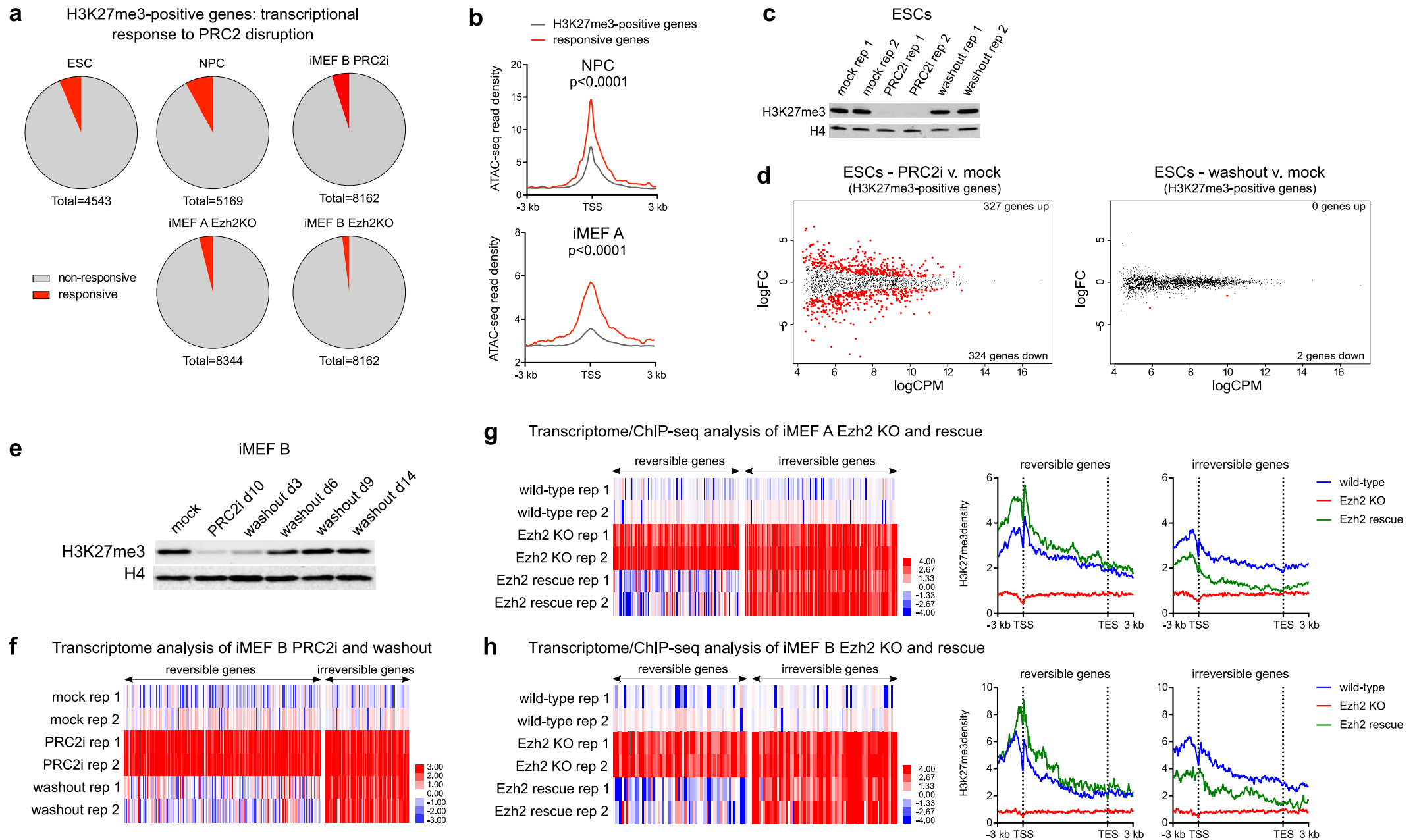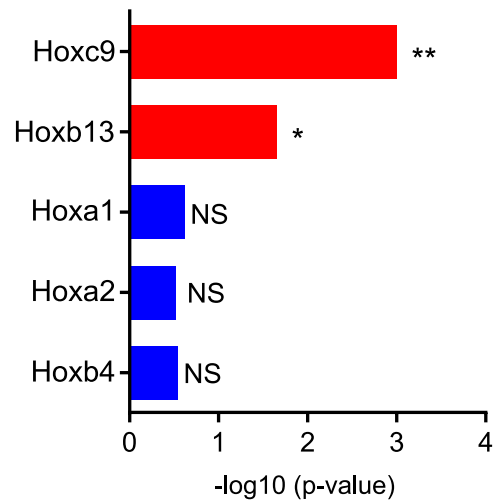
Extended Data Fig. 3. Transient disruption of PRC2 triggers permanent activation of a large subset of repressed target genes in differentiated somatic cells. a, Relative proportions of non-responsive and responsive genes among the indicated totals of genes whose transcription start site overlaps a H3K27me3 peak, in NPCs, ESCs and iMEF line B after treatment with PRC2 inhibitors and washout, and in iMEF lines A and B after genetic deletion of Ezh2 followed by Ezh2 rescue. H3K27me3 profiles in ESCs were determined from a published data set[26]. NPC, mouse neural progenitor cells. ESC, mouse embryonic stem cells. iMEF, immortalized mouse embryonic fibroblasts. **b,** Metaplots of average ATAC-seq density over the interval from TSS -/+ 3 kb for the full sets of H3K27me3-positive and transcriptionally responsive PRC2 target genes in NPC[36] and iMEF A (this study). **c,** Western blot analysis of nuclear extracts from the indicated conditions. PRC2i, PRC2 inhibition with 2 μM UNC1999 and 4 μM A-395. **d,** MA plots comparing RNA-seq levels of H3K27me3-positive genes in ESCs cultured in the presence of PRC2 inhibitors, or after washout of the inhibitors, to mock-treated cells. CPM, counts per million. FC, fold change. Significantly differentially expressed genes (Benjamini-Hochberg-adjusted p < 0.05) are indicated in red. **e,** Western blot analysis of nuclear extracts from the indicated conditions. **f,** Heatmap of RNA-seq levels (log2 fold change with respect to the mean of the two mock replicates) in the indicated conditions for the full sets of reversible and irreversible PRC2 target genes in iMEF B. **g,** Left, heatmap of RNA-seq levels (log2 fold change with respect to the mean of the two wild-type replicates) in the indicated conditions for the full sets of reversible and irreversible PRC2 target genes in iMEF A. Right, metaplots of average H3K27me3 ChIP-seq density over the interval from TSS − 3 kb to TES + 3 kb for the full sets of reversible and irreversible PRC2 target genes in iMEF A in the indicated conditions. TSS, transcription start site. TES, transcription end site. **h,** As in **g** but in iMEF B.
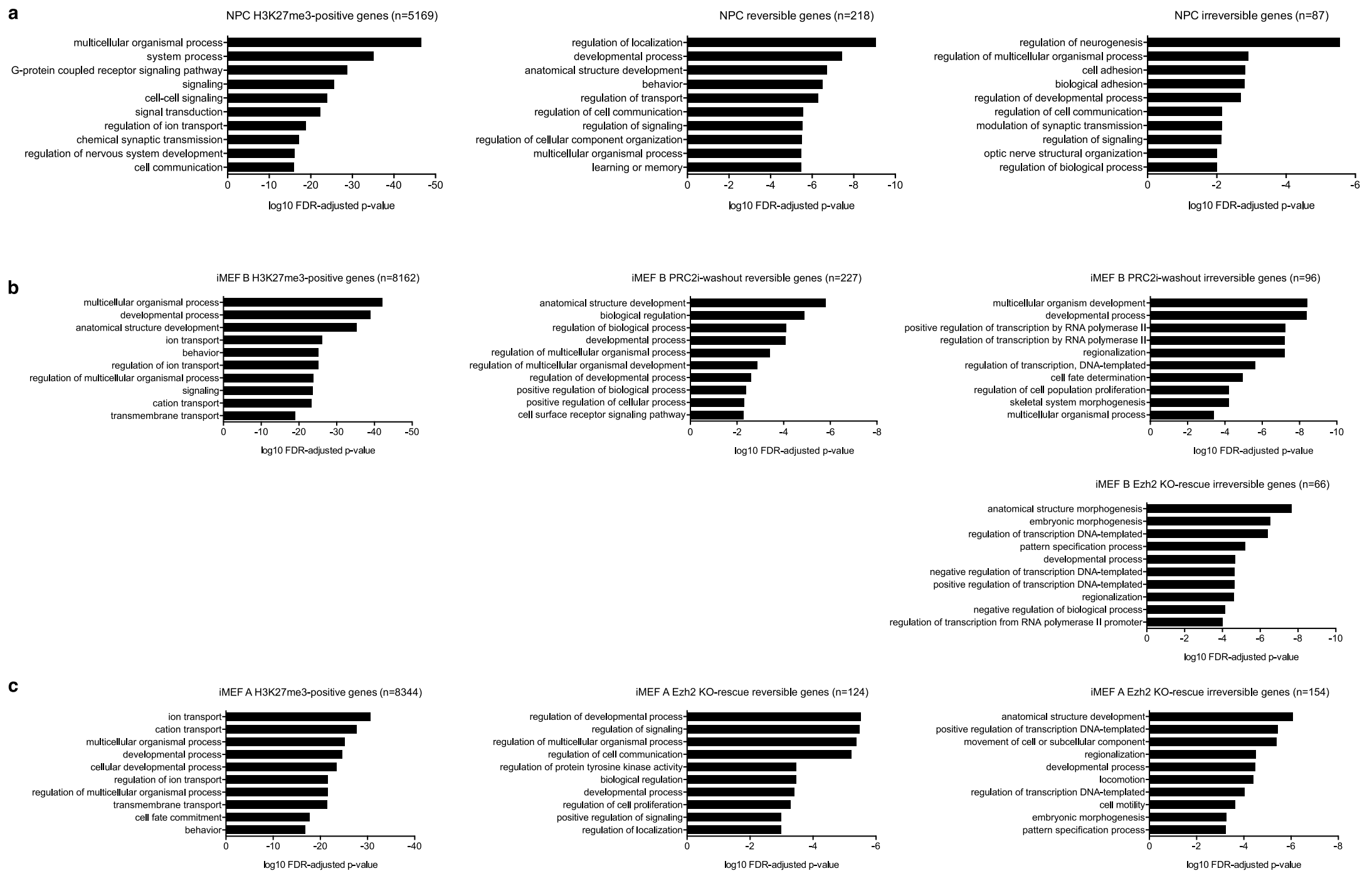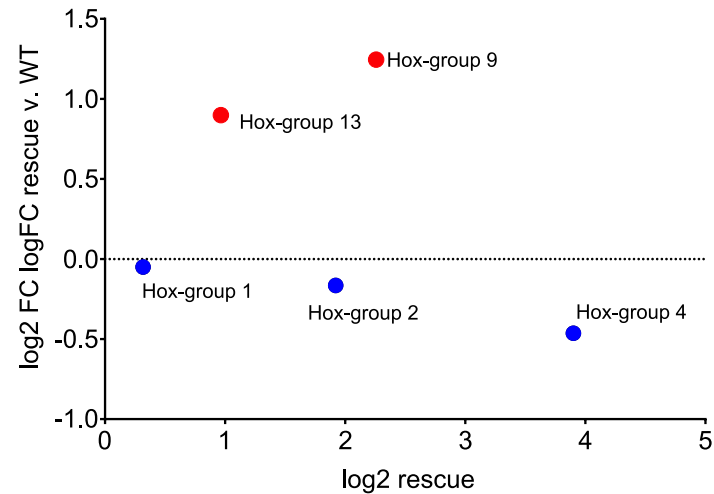
Extended Data Fig. 4. Reversible and irreversible PRC2 targets are similarly enriched in gene ontology terms related to development. a, Left, top 10 most highly enriched gene ontology (GO) terms among genes whose transcription start site overlaps an H3K27me3 peak in NPCs, using all mouse genes as background, with FDR-adjusted p-value indicated for each term. Right, top 10 most highly enriched GO terms among reversible and irreversible genes in NPCs, respectively, as indicated, using all mouse genes as background, with FDR-adjusted p-value indicated for each term. **b**, As in **a** but for iMEF B subjected to transient PRC2i treatment (top panels) or Ezh2 deletion and rescue (bottom panel, no significantly enriched GO term was found for reversible genes). PRC2i, PRC2 inhibition with 2 μM UNC1999 and 4 μM A-395. **c**, As in **a**, but for iMEF A.
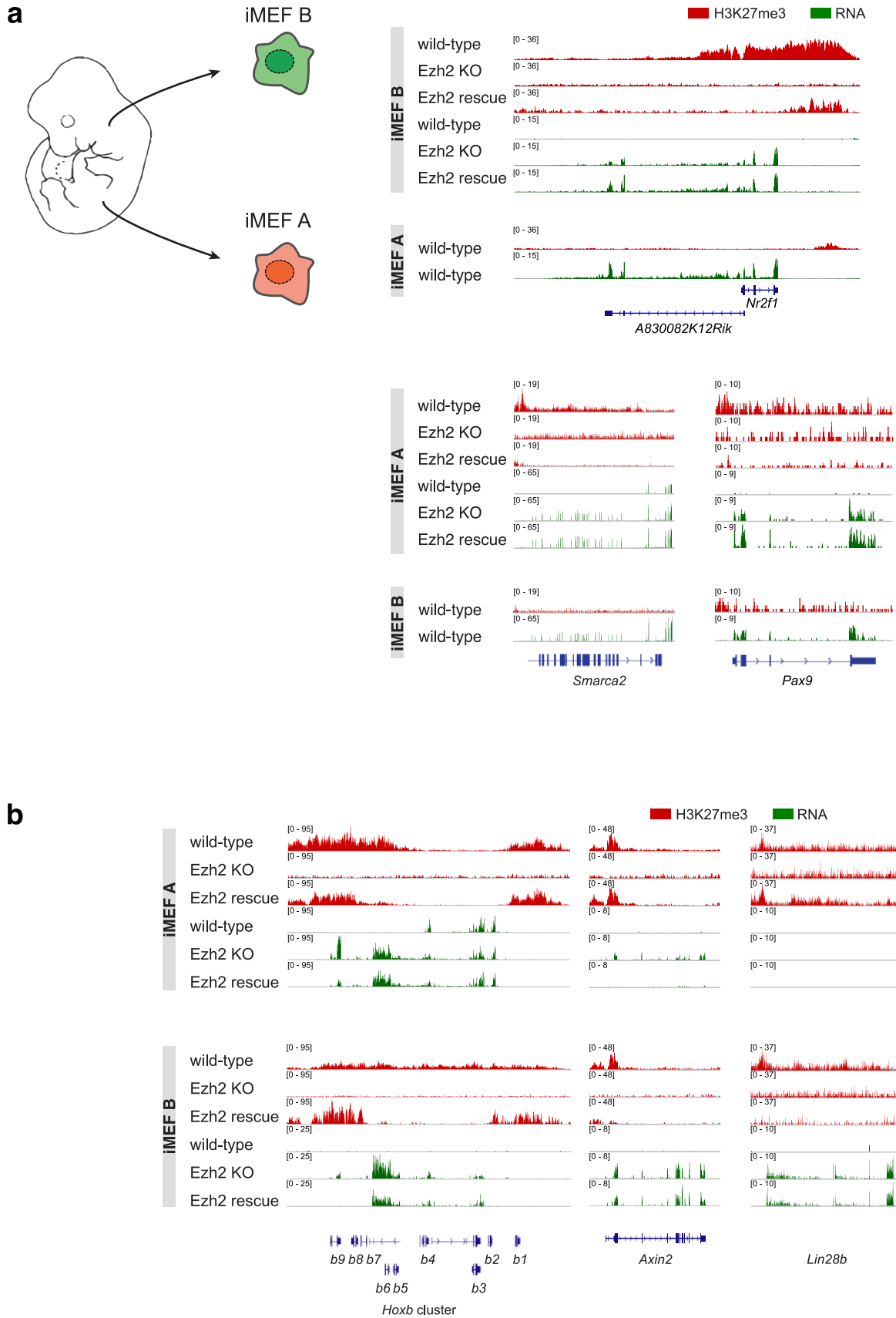
a iMEF A - ATAC-seq
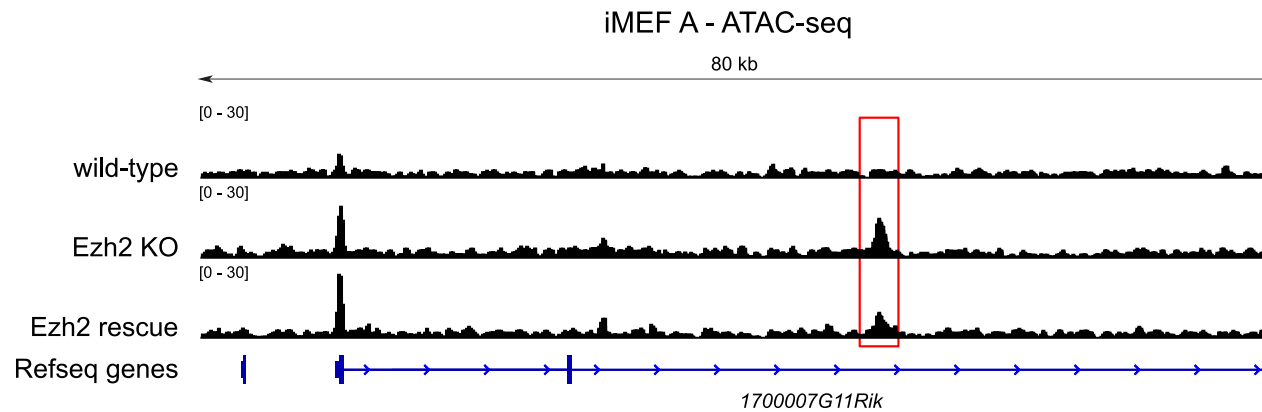
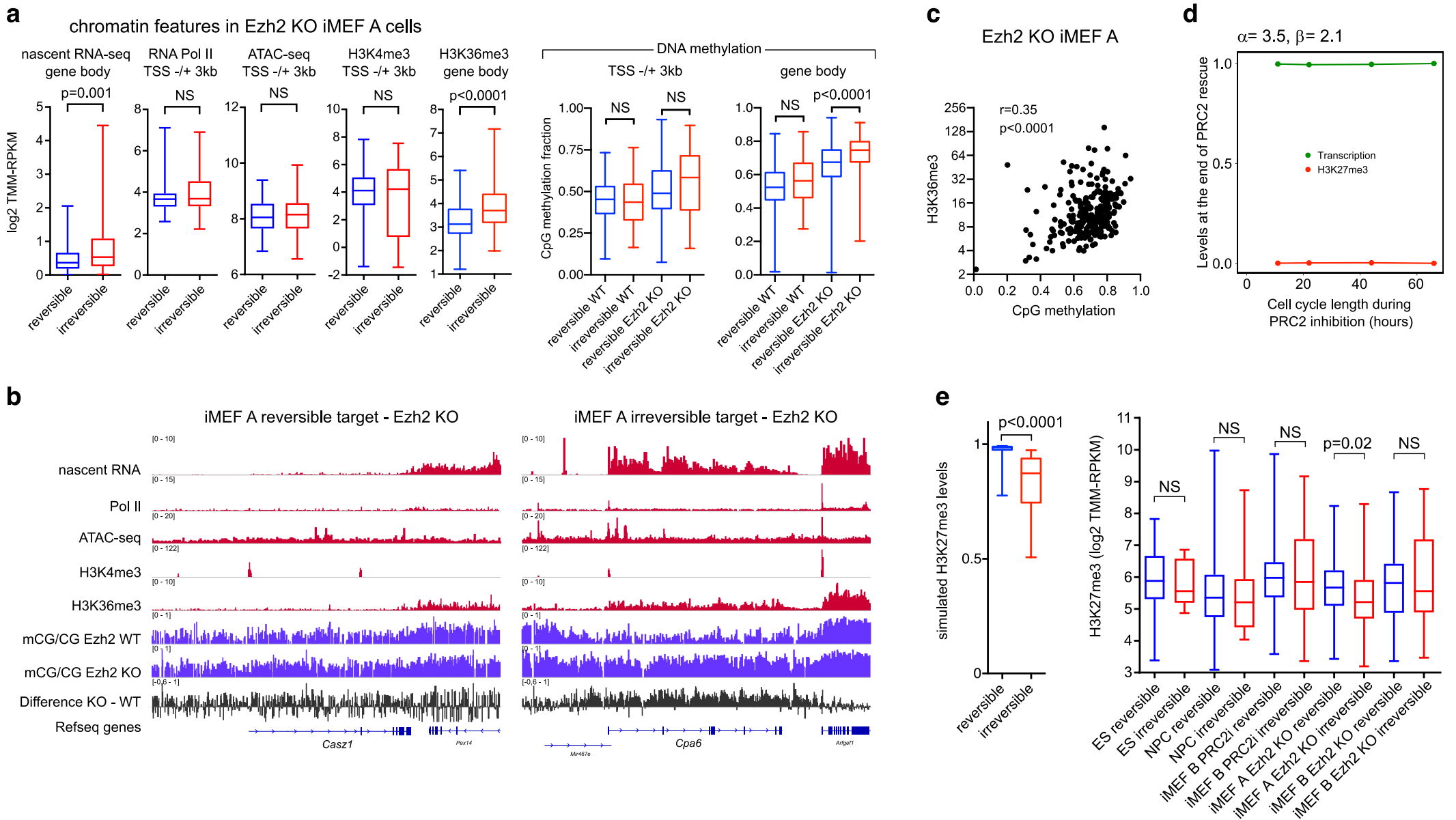**b** iMEF A - irreversible ATAC-seq peaks > focus on Hox motifs

**c** iMEF A - Hox paralogous group differential expression (mean TMM-RPKM RNA-seq)

Extended Data Fig. 5. Disruption of PRC2 activity in iMEFs triggers widespread genomic binding of de-repressed homeotic transcription factors. a, Tracks of ATAC-seq performed in the indicated genotypes. Red box highlights a peak irreversibly gained following temporary deletion of Ezh2. ATAC, Assay for Transposase-Accessible Chromatin. **b,** Results of mammalian Hox factors among total known motif search using HOMER software, on the indicated peaks called using SEACR, and with all Ezh2 KO peaks as background (* denotes a q-value < 0.05, ** denotes a q-value < 0.005). See also Extended Data Table 2. NS, not significant. **c,** Normalized RNA-seq counts in iMEF A were averaged members of each Hox paralogous group 1, 2, 4, 9 and 13, and the fold derepression in Ezh2 rescue versus wild-type was plotted against the expression level in Ezh2 rescue. Hox-group 9 and 13 are colored in red to highlight the combination of their high fold upregulation and high expression. TMM-RPKM, trimmed mean of M-values-reads per kilobase per million. FC, fold change.

Extended Data Fig. 6. Stable epigenetic switching of PRC2 targets is not a gene-intrinsic property. a, Left, schematic illustrating the heterogeneous identity of distinct MEF clones. Right, tracks of H3K27me3 ChIP-seq and RNA-seq for the indicated conditions over individual genes comparing iMEF A and iMEF B. **b**, Tracks of H3K27me3 ChIP-seq and RNA-seq for the indicated conditions over individual genes or regions comparing iMEF A and iMEF B.

Extended Data Fig. 7. Stable epigenetic switching of target genes is correlated to level of transcriptional activity upon disruption of PRC2. a, Box plots (median, lower and upper quartiles, lowest and highest values) of average nascent RNA-seq read densities, ChIP-seq read densities measured for the indicated chromatin features, ATAC-seq densities and fraction of CpG methylation. For nascent RNA, Pol II, ATAC-seq, H3K4me3 and H3K36me3, p-values are the results of Mann-Whitney tests comparing irreversible and reversible genes for each feature. Difference in nascent RNA (Hodges-Lehmann): 0.15; confidence interval: 0.05 to 0.27. Difference in H3K36me3 (Hodges-Lehmann): 0.56; confidence interval: 0.39-0.76. For DNA methylation, p-values are the results of a Kruskal-Wallis test. Mean rank difference for reversible Ezh2 KO v. irreversible Ezh2 KO: -88.90. TSS = transcription start site. NS, not significant. TMM-RPKM, trimmed mean of M-values-reads per kilobase per million. **b,** Genomic tracks for the indicated chromatin features at representative reversible and irreversible PRC2 target genes in iMEF A Ezh2 KO cells. **c,** Scatter plot of all reversible and irreversible genes according to their fraction of methylated CpG and log2 TMM-RPKM H3K36me3 ChIP-seq read density. Spearman's rank correlation coefficient and corresponding p-value are indicated. **d,** Graph depicting the levels of transcription (fraction of level reached in case with 20 cell cycles of transient PRC2 disruption), and H3K27me3 levels, predicted at the conclusion of a simulation similar to that conducted for Fig. 3d (top) for the indicated α, β values. Transient disruption of PRC2 was simulated for a fixed duration (corresponding to that of Fig. 3d) with varying cell cycle lengths, followed by 20 cell cycles of normal duration during which PRC2 activity was restored, and levels of transcription and H3K27me3 at 20th cell cycle were plotted. **e,** Left, box plots comparing H3K27me3 levels of all simulated genes predicted to exhibit reversible or irreversible de-repression, respectively. The levels are from the wild-type simulations in Fig. 3b (left), with parameter values sampled logarithmically over parameter space (see Methods). Difference (Hodges-Lehmann): 0.10; confidence interval: 0.01-0.12. Right, box plots of observed H3K27me3 levels over all reversible and irreversible genes, respectively, in the indicated cell lines under wild-type untreated conditions. p-values are the results of Mann–Whitney tests comparing irreversible and reversible genes for each cell line. Difference in H3K27me3 for iMEF A (Hodges-Lehmann): 0.45; confidence interval: 0.14-0.58. PRC2i, PRC2 inhibition with 2 μM UNC1999 and 4 μM A-395.
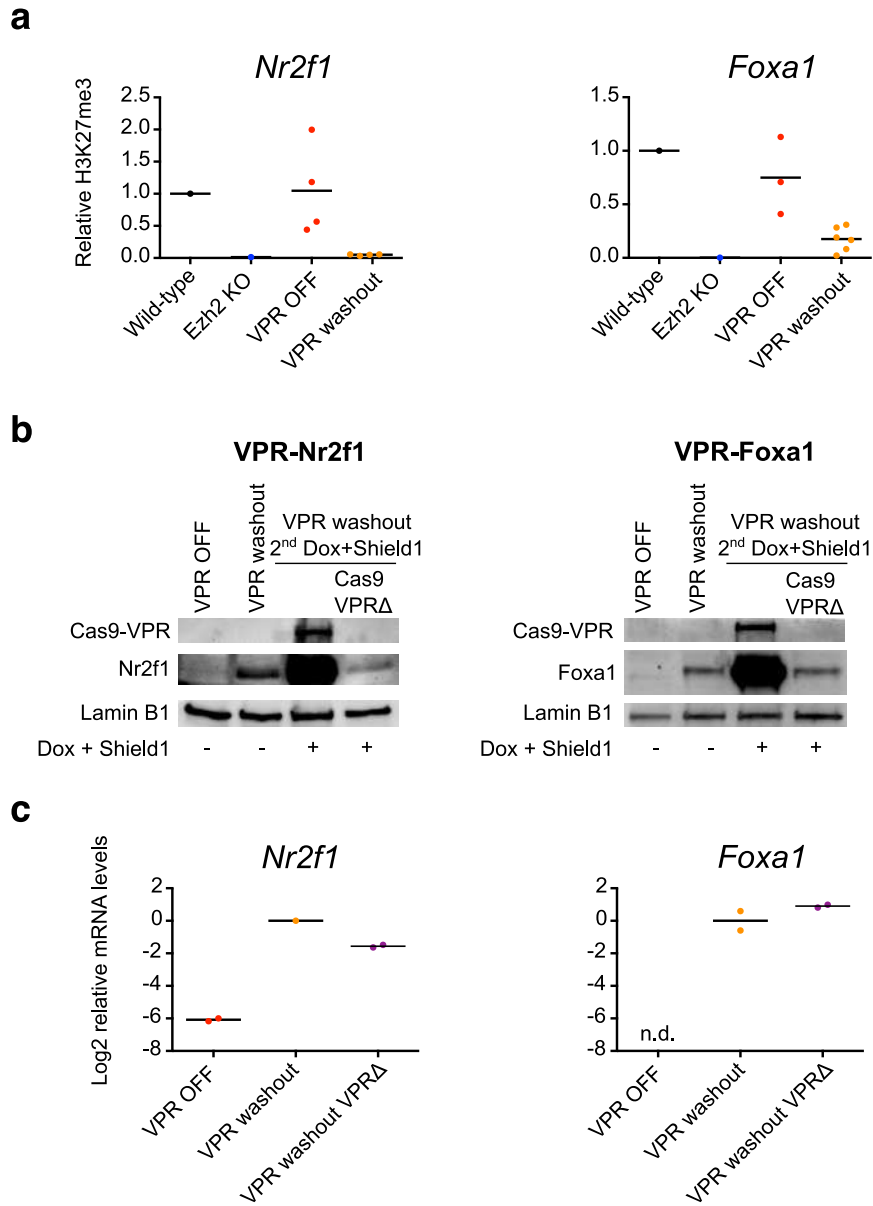
Extended Data Fig. 8. Transient activation of individual PRC2 target genes can trigger permanent switching of transcriptional states. a, H3K27me3 levels measured by CUT&RUN over indicated target genes in cells bearing the DD-dCas9-VPR construct and either lacking (wild-type, Ezh2 KO) or constitutively expressing (VPR OFF, washout) sgRNAs specific to the target gene. Values within each experiment are normalized to the wild-type condition. Horizontal lines represent mean values. **b**, Western blot analysis of nuclear extracts from the indicated conditions. Cells having undergone a transient induction experiment, and a subclone thereof in which DD-dCas9-VPR was genetically deleted, were subjected to a second Dox+Shield1 treatment to confirm the deletion and check the persistence of target gene product expression. **c**, Messenger RNA levels of indicated target genes in cells constitutively expressing sgRNAs specific to the target gene and either bearing the DD-dCas9-VPR construct or deleted for DD-dCas9-VPR after the conclusion of a transient induction experiment. Values within each experiment are normalized to the VPR washout condition. n.d., not detected.
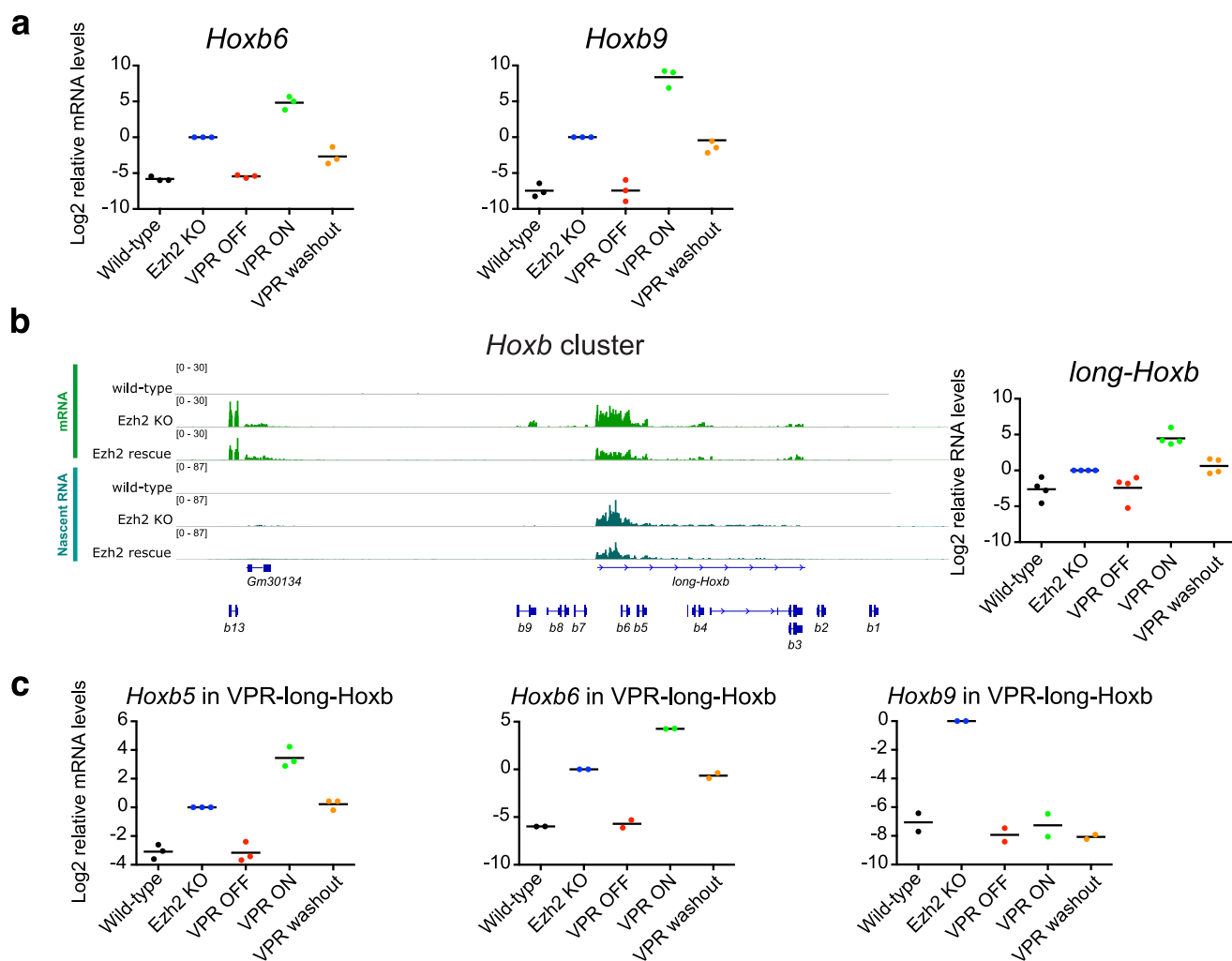
Extended Data Fig. 9. *Hoxb* cluster genes exhibit interdependent switching of transcriptional states in response to transient activation. a, Messenger RNA levels of indicated target genes in cells bearing the DD-dCas9-VPR construct and either lacking (wild-type, Ezh2 KO) or constitutively expressing (VPR OFF, ON, washout) sgRNAs specific to the target gene. Values within each experiment are normalized to the Ezh2 KO condition. Horizontal lines represent mean values. **b**, Left, RNA-seq and nascent-RNA-seq over the *Hoxb* cluster for the indicated conditions in iMEF B, with the position of the *long-Hoxb* transcript shown below. Right, as in **a**, but for *long-Hoxb*. **c**, Messenger RNA levels of indicated target genes in cells bearing the DD-dCas9-VPR construct and either lacking (wild-type, Ezh2 KO) or constitutively expressing (VPR OFF, ON, washout) sgRNAs specific to *long-Hoxb*.
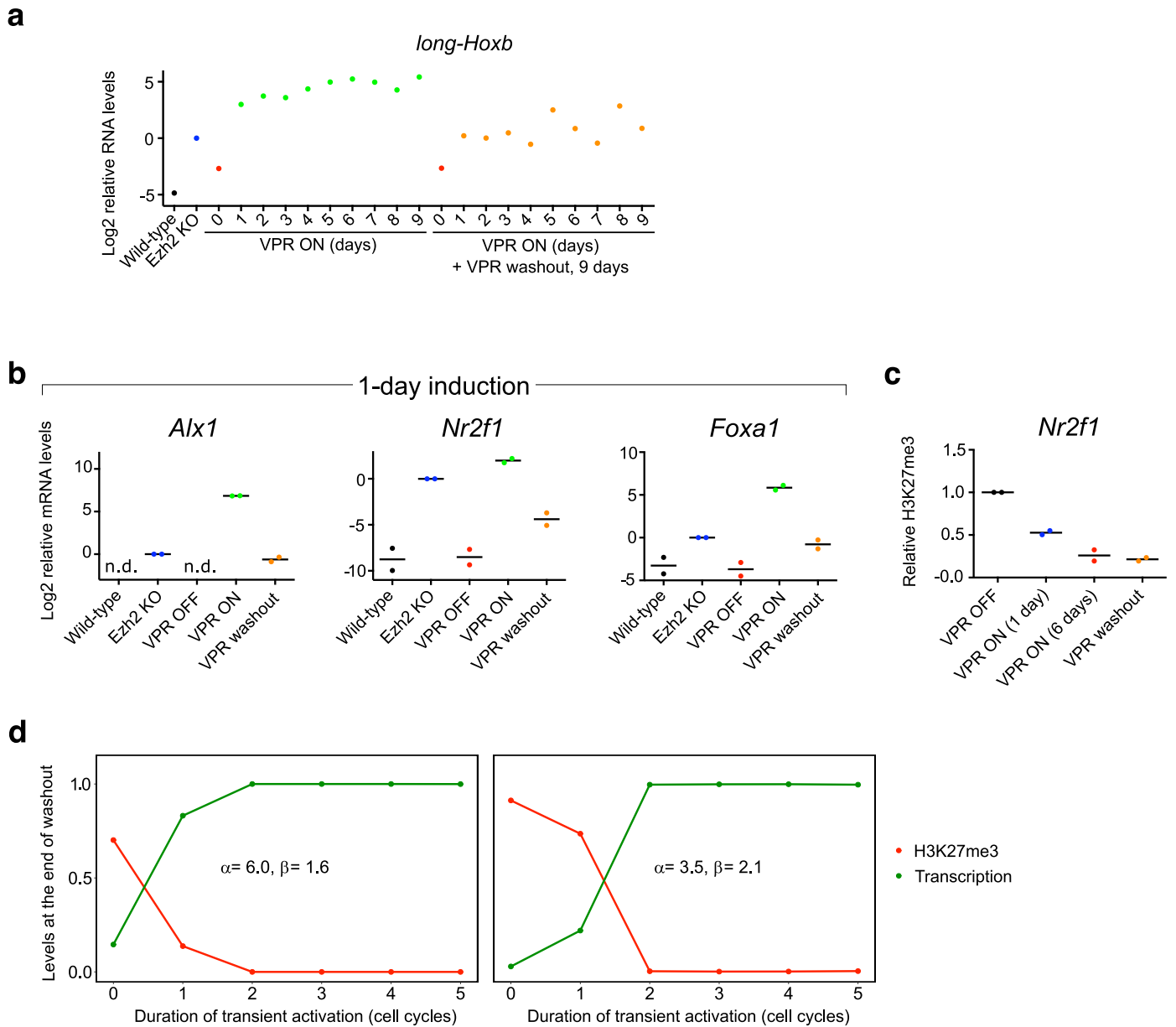
Extended Data Fig. 10. Short pulses of transient activation can suffice to produce a switch in transcriptional states. a, Messenger RNA levels of *long-Hoxb* in cells bearing the DD-dCas9-VPR construct and either lacking (wild-type, Ezh2 KO) or constitutively expressing (VPR ON, washout) sgRNAs specific to *long-Hoxb*, after induction for the indicated duration followed or not by 9-day washout. Values are normalized to the Ezh2 KO condition. **b**, Messenger RNA levels of indicated target genes in cells bearing the DD-dCas9-VPR construct and either lacking (wild-type, Ezh2 KO) or constitutively expressing (VPR OFF, ON, washout) sgRNAs specific to the target gene. Values within each experiment are normalized to the Ezh2 KO condition. Horizontal lines represent mean values. n.d., not detected. **c**, H3K27me3 levels measured by CUT&RUN over *Nr2f1* in cells bearing the DD-dCas9-VPR construct, constitutively expressing sgRNAs specific to *Nr2f1*, and subjected to the indicated conditions. VPR washout condition follows a 6-day induction. Values within each experiment are normalized to the VPR OFF condition. **d**, Graphs depicting the levels of transcription (fraction of the maximum level reached for the indicated α, β values), and H3K27me3 levels, predicted at the conclusion of a simulation similar to that conducted for Fig. 3d. A transient pulse of transcriptional activation with α = α$_{max}$ = 100 was simulated for the indicated number of cell cycles, followed by 20 cell cycles at the indicated α, β values, and levels of transcription and H3K27me3 at 20th cell cycle were plotted.
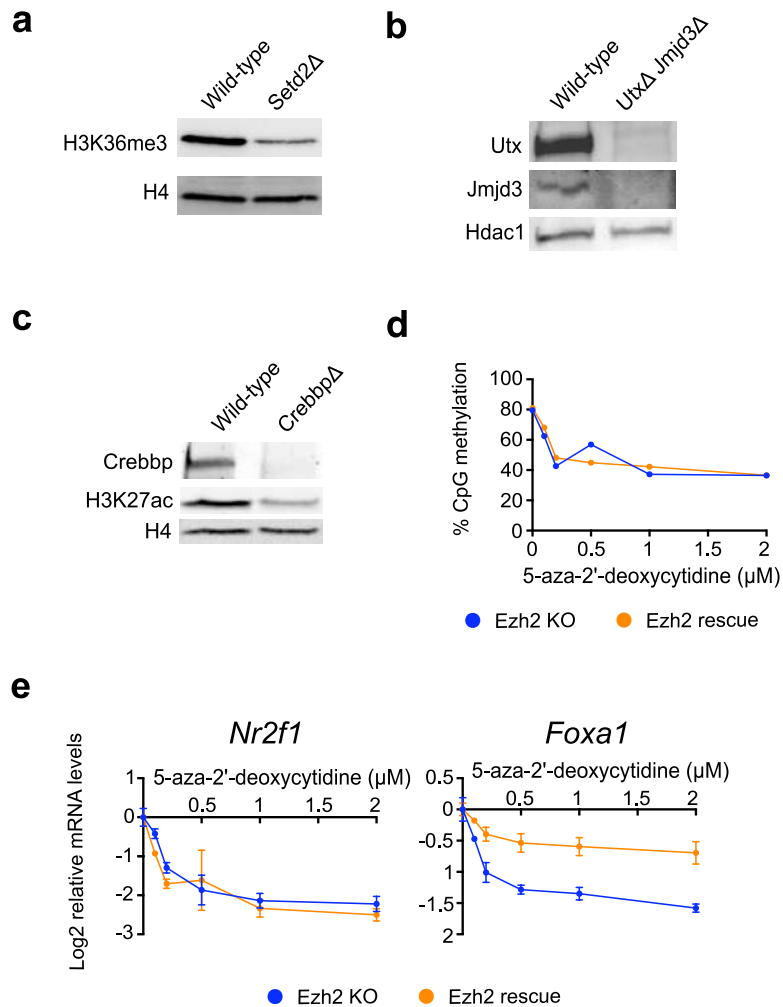
Extended Data Fig. 11. Stable switching of transcriptional states can occur independently of Setd2, of Utx and Jmjd3, and of Crebbp, and global loss of DNA methylation does not restore PRC2-dependent silencing. a, **b**, **c**, Western blot analysis of nuclear extracts from iMEF B cells of the indicated genotypes. **d**, Global levels of CpG methylation measured by LUminometric Methylation Assay in iMEF B cells of the indicated genotypes after treatment for three days with different concentrations of 5-aza-2'-deoxycytidine as shown. **e**, Messenger RNA levels of indicated target genes in cells of the indicated genotypes after treatment for three days with different concentrations of 5-aza-2'-deoxycytidine as shown.
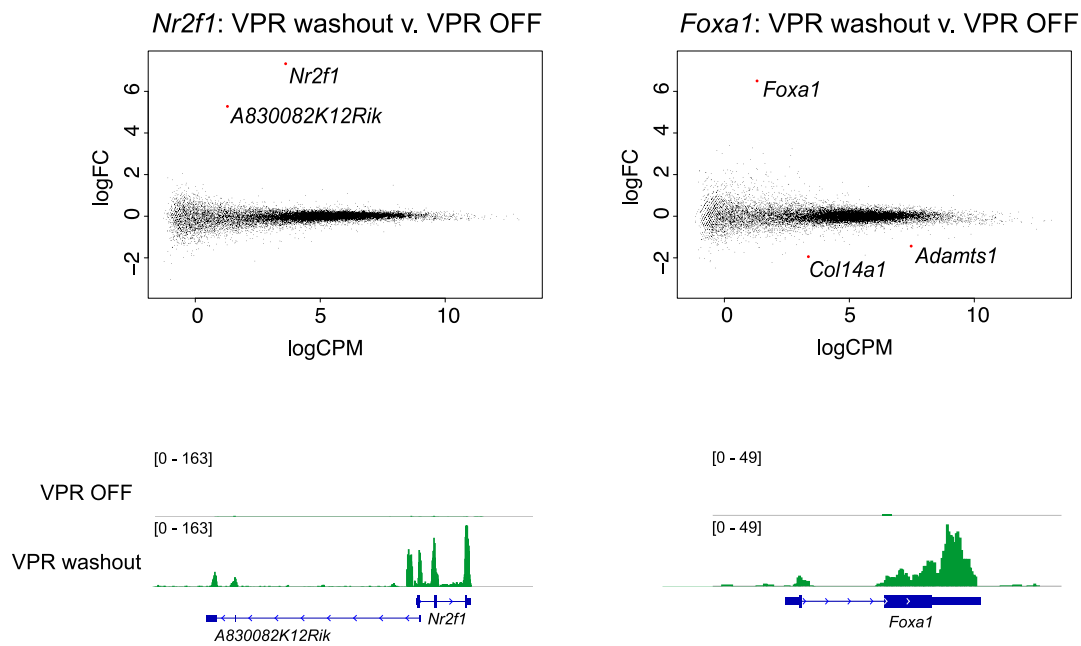
Extended Data Fig. 12. Switching of transcriptional states following transient activation can be gene-autonomous. Top, MA plots comparing RNA-seq levels in cells in which the indicated gene was subjected to transient activation as depicted in Fig. 4a (VPR washout) to levels in control untreated cells (VPR OFF). CPM, counts per million. FC, fold change. Significantly differentially expressed genes (Benjamini-Hochberg-adjusted p < 0.05) are indicated in red. *A830082K12Rik* is transcribed divergently from a common promoter region shared with *Nr2f1*. Bottom, RNA-seq tracks for the indicated conditions at transiently activated genes.